

Structured Linear CDEs: Maximally Expressive and Parallel-in-Time Sequence Models

Benjamin Walker
 Mathematical Institute
 University of Oxford

Lingyi Yang
 Mathematical Institute
 University of Oxford

Nicola Muca Cirone
 Department of Mathematics
 Imperial College London

Cristopher Salvi
 Department of Mathematics
 Imperial College London

Terry Lyons
 Mathematical Institute
 University of Oxford

Abstract

Structured Linear Controlled Differential Equations (SLiCEs) provide a unifying framework for sequence models with structured, input-dependent state-transition matrices that retain the maximal expressivity of dense matrices whilst being cheaper to compute. The framework encompasses existing architectures, such as input-dependent block-diagonal linear recurrent neural networks and DeltaNet’s diagonal-plus-low-rank structure, as well as two novel variants based on sparsity and the Walsh–Hadamard transform. We prove that, unlike the diagonal state-transition matrices of S4 and Mamba, SLiCEs employing block-diagonal, sparse, or Walsh–Hadamard matrices match the maximal expressivity of dense matrices. Empirically, SLiCEs solve the A_5 state-tracking benchmark with a single layer, achieve best-in-class length generalisation on regular language tasks among parallel-in-time models, and match the state-of-the-art performance of log neural controlled differential equations on six multivariate time-series classification datasets while cutting the average time per training step by a factor of twenty.

1 Introduction

Parallel-in-time architectures, such as Transformers and Structured State-Space Models (SSMs), have allowed language models to scale to billions of parameters [89, 34]. However, theory and practice agree that these models do not generalise to longer sequences on state-tracking problems, a task that classical recurrent neural networks (RNNs) handle with ease [58, 59, 54]. Reframing SSMs as Linear Neural Controlled Differential Equations (LNCDEs), it becomes clear that using a diagonal state-transition matrix severely restricts expressivity [18]. Replacing it with a dense matrix restores maximal expressivity and the ability to state-track, but increases the number of parameters and computational cost from $\mathcal{O}(d_h^2)$ to $\mathcal{O}(d_h^3)$, where d_h is the hidden dimension [59, 18].

Structured alternatives seek the best of both worlds. Block-diagonal Linear RNNs (LRNNs) [28] and the Diagonal-Plus-Low-Rank (DPLR) structure of DeltaNet [77, 94, 80] reduce computational cost while preserving some expressivity, with the latter recently shown to be maximally expressive [65]. We generalise and extend these ideas with Structured Linear Controlled Differential Equations (SLiCEs), a general framework for structured, input-dependent state-transition matrices.

Contributions

1. Structured Linear Controlled Differential Equations (SLiCEs) are introduced as a common lens for models with structured, input-dependent state-transition matrices. This framework incorporates SSMs such as Mamba [34], LRNNs such as DeltaNet [77] and input-dependent block-diagonal LRNN [28], LNCDEs [18], and two novel structures based on sparse matrices and the Walsh–Hadamard transform.

2. Block-diagonal, sparse, and Walsh–Hadamard SLiCEs are proven to achieve maximal probabilistic expressivity in Theorems 4.1, 4.2, and 4.3, respectively. Previously, such expressivity had only been shown for dense and DPLR matrices [18, 65].
3. A comprehensive empirical evaluation showing that the structure of the state-transition matrix significantly impacts length generalisation on state-tracking problems. The block-diagonal structure emerges as a promising option, due to its strong empirical results and favourable parallelisation. Furthermore, on six real-world multivariate time-series classification datasets, a block-diagonal SLiCE is shown to match the predictive accuracy of Log-NCDEs, whilst reducing the per-step training time by a factor of 20.
4. Open-source implementations of SLiCEs in both PyTorch and JAX, along with code to fully reproduce all experiments from this paper. These are available at <https://github.com/Benjamin-Walker/structured-linear-cdes> (PyTorch) and <https://github.com/Benjamin-Walker/log-neural-cdes> (JAX).

Related work Increasing the expressivity of parallel-in-time sequence models while retaining their computational efficiency is of significant interest to the sequence modelling community, as it would facilitate training large, performant models. One approach parallelises non-linear RNNs by rewriting them as fixed-point problems and applying parallel Newton or quasi-Newton methods to calculate their output [53, 31]. However, reported wall-clock gains remain limited; parallel autoregressive generation can be up to twice as slow as sequential baselines [31]. There have also been large numbers of input-dependent LRNN architectures proposed, including input-dependent block-diagonal LRNN [28], DeltaNet [93], DeltaProduct [80], Gated DeltaNet [94], Mamba [34], Mamba-2 [24], RWKV-7 [69], HGRN-2 [71], mLSTM [6], Gated Linear Attention [92], Gated Random Feature Attention [70], Gated Slot Attention [95], TTT-Linear [85], and Titans [7]. All of these model use either diagonal or DPLR state-transition matrices, and a comparison of individual architectures for a number of these models can be found in Table 2 of [93].

Utilising structured matrices to reduce the computational burden of neural networks extends beyond sequence models. Sparsity is motivated by the lottery-ticket hypothesis [30] and has been realised through pruning before [84], during [87], and after training [38]. Other examples of structured matrices in neural network architectures include sparse Transformers [14], 2 : 4 sparse linear layers [60], and Monarch layers, which are the product of two block-diagonal matrices [25].

2 Background

2.1 Linear controlled differential equations

Let $\omega : [0, T] \rightarrow \mathbb{R}^{d_\omega}$ be a path with bounded-variation. A linear controlled differential equation takes the form

$$dh_s = \sum_{i=1}^{d_\omega} A^i h_s d\omega_s^i, \quad (1)$$

where $A^i \in \mathbb{R}^{d_h \times d_h}$ is the linear vector field for each channel $i = 1, \dots, d_\omega$, and $h : [0, T] \rightarrow \mathbb{R}^{d_h}$ is the solution path. Approximating ω_s with linear interpolation on the grid $0 = t_0 < \dots < t_n = T$ yields

$$\tilde{h}_{t_{j+1}} = \exp \left(\sum_{i=1}^{d_\omega} (\omega_{t_{j+1}}^i - \omega_{t_j}^i) A^i \right) \tilde{h}_{t_j}. \quad (2)$$

The outputs \tilde{h}_{t_j} are then computable in $\mathcal{O}(\log(n))$ parallel steps by composing the flow on each interval using an associative parallel scan [8]. This approach has been used to parallelise linear RNNs [57] and SSMs [81].

On each interval $[t_j, t_{j+1}]$, (2) uses a first-order approximation of the linear CDE. The Log-ODE method extends this to higher orders by combining the iterated Lie brackets of the vector field with the log-signature of ω [12]. See Cass and Salvi [11, Section 3.2.2] for a summary description of the algorithm and Appendix B for a description of applying the algorithm to a linear neural controlled differential equation.

2.2 Linear neural controlled differential equations

Let $\{(t_i, x_i)\}_{i=0}^n$ denote a set of observations from a multivariate time-series and $X : [t_0, t_n] \rightarrow \mathbb{R}^{d_X}$ be a continuous interpolation, such that $X_{t_i} = (t_i, x_i)$. Neural Controlled Differential Equations (NCDEs) are defined as

$$h_{t_0} = \xi_\phi(t_0, x_0), \quad h_t = h_{t_0} + \int_{t_0}^t g_\theta(h_s) dX_s, \quad z_t = l_\psi(h_t), \quad (3)$$

where $\xi_\phi : \mathbb{R}^{d_X} \rightarrow \mathbb{R}^{d_h}$ and $g_\theta : \mathbb{R}^{d_h} \rightarrow \mathbb{R}^{d_h \times d_X}$ are neural networks, and $l_\psi : \mathbb{R}^{d_h} \rightarrow \mathbb{R}^{d_z}$ is a linear map [48]. NCDEs have a number of desirable properties, including maximal expressivity and robustness to irregular sampling rates. Building on the work of Neural Rough Differential Equations [63], Log-NCDEs [91] demonstrate that combining NCDEs with the Log-ODE method during training leads to state-of-the-art performance on a range of multivariate time-series modelling benchmarks with up to 50,000 observations.

A Linear NCDE (LNCDE) takes the form

$$h_t = h_{t_0} + \int_{t_0}^t \sum_{i=1}^{d_\omega} A_\theta^i h_s d\omega_s^{X,i} = h_{t_0} + \int_{t_0}^t \left(\sum_{i=1}^{d_\omega} A_\theta^i d\omega_s^{X,i} \right) h_s, \quad (4)$$

where $\omega^X : [t_0, t_n] \rightarrow \mathbb{R}^{d_\omega}$ is a path which depends on the input X and the A_θ^i are trainable matrices. As will be discussed further in Section 3.2, LNCDEs are maximally expressive [48, 18]. Therefore, there exists a maximally expressive sequence model whose recurrence can be calculated parallel-in-time using the approach outlined in Section 2.1. However, the number of parameters and computational cost makes the modification infeasible in large models. Independently of LNCDEs, Merrill et al. [59] proposed IDS4, a modification of the S4 layer designed to allow state-tracking, which has the same form as (4).

This paper focuses on LNCDEs with vector-valued hidden states. In practice, however, LRNNs such as Mamba and DeltaNet typically employ matrix-valued hidden states. Appendix C outlines how LNCDEs (and hence SLiCEs) can be naturally extended to this setting via n parallel vector-valued LNCDEs, with theoretical results and parallelisability carrying over unchanged.

3 Expressivity

3.1 Introduction

Expressivity characterises the set of functions a model can approximate, and maximal expressivity (or universal approximation) guarantees that, with suitable parameters, any continuous function on a compact set can be approximated arbitrarily closely.

Definition 3.1 (Maximal expressivity). Let \mathcal{X} be a topological space, and let $\mathcal{F} = \{f_\theta : \mathcal{X} \rightarrow \mathbb{R} \mid \theta \in \Theta\}$ be a class of real-valued functions on \mathcal{X} , parametrised by some set Θ . We say that \mathcal{F} is maximally expressive (or universal) if, for every compact set $\mathcal{K} \subset \mathcal{X}$ and every real-valued continuous function $f : \mathcal{K} \rightarrow \mathbb{R}$, the following property holds:

$$\forall \epsilon > 0, \exists \theta \in \Theta \quad \text{s.t.} \quad \sup_{x \in \mathcal{K}} |f(x) - f_\theta(x)| < \epsilon. \quad (5)$$

A classical result is the Universal Approximation Theorem, which states that when $\mathcal{X} = \mathbb{R}^d$, the class \mathcal{F} of single-hidden-layer feed-forward networks with a suitable activation function is maximally expressive [23, 42].

3.2 Maximally expressive models on paths

Let \mathcal{X} denote the space of continuous paths of bounded variation on the interval $[0, T]$ which all begin at the same point and contain time as a channel (time-augmented). We endow this space with the 1-variation topology. Let \mathcal{F} be the class of LNCDEs defined in (4) with a linear readout layer l_{θ_2} , such that $f_\theta : \mathcal{X} \rightarrow \mathbb{R}$ is defined by

$$\omega \mapsto l_{\theta_2}(h_{t_n}) = l_{\theta_2} \left(h_{t_0} + \int_{t_0}^{t_n} \sum_{i=1}^{d_\omega} A_{\theta_1}^i h_s d\omega_s^i \right), \quad (6)$$

for $\omega \in \mathcal{X}$. In this setting, \mathcal{F} is maximally expressive [45]. Furthermore, LNCDEs with diagonal matrices $A_{\theta_1}^i$, i.e. S4 [35] and Mamba [34], are not maximally expressive [18]. An alternative to maximal expressivity is the following probabilistic property.

Definition 3.2 (Maximal Probabilistic Expressivity). Let \mathcal{X} be a topological space, $N \in \mathbb{N}$, and $\mathcal{F}^N = \{f_\theta^N : \mathcal{X} \rightarrow \mathbb{R} \mid \theta \in \Theta^N\}$ be a class of real-valued functions on \mathcal{X} defined by

$$f_\theta^N(\omega) = l_{\theta_2}(\tilde{f}_{\theta_1}^N(\omega)), \quad (7)$$

for $\omega \in \mathcal{X}$, where $\tilde{f}_{\theta_1}^N : \mathcal{X} \rightarrow \mathbb{R}^N$, $l_{\theta_2} \in \mathbb{R}^N$ is a linear readout, $\theta_1 \in \Theta_1^N$, $\theta_2 \in \Theta_2^N$, and $\Theta^N = \Theta_1^N \cup \Theta_2^N$. Given a sequence of probability measures \mathbb{P}_N on Θ_1^N with $\theta_1 \sim \mathbb{P}_N$, \mathcal{F} has maximal probabilistic expressivity if, for every compact set $\mathcal{K} \subset \mathcal{X}$ and every real-valued continuous function $f : \mathcal{K} \rightarrow \mathbb{R}$, the following property holds:

$$\lim_{N \rightarrow \infty} \mathbb{P}_N \left\{ \exists l_{\theta_2} \text{ s.t.} \sup_{\omega \in \mathcal{K}} |f(\omega) - f_\theta^N(\omega)| < \epsilon \right\} = 1. \quad (8)$$

In the context of machine learning, maximal probabilistic expressivity may be considered a more promising property than maximal expressivity, as for large enough N , it implies there exists a significant abundance of parameters θ_1 that are capable of achieving uniformly bounded and arbitrarily low error rates with a linear readout layer. These parameters should therefore be readily discoverable through classical optimisation methods.

In the case of LNCDEs, $N = d_h$,

$$\tilde{f}_{\theta_1}^{d_h}(\omega) = h_{t_0} + \int_{t_0}^{t_n} \sum_{i=1}^{d_\omega} A_{\theta_1}^i h_s d\omega_s^i, \quad (9)$$

and \mathbb{P}_{d_h} on $\Theta_1^{d_h}$ is a collection of probabilities on matrices $\mathbb{P}_{d_h}^i$ with $A_{\theta_1}^i \sim \mathbb{P}_{d_h}^i$. Achieving maximal probabilistic expressivity depends crucially on the choice of $\mathbb{P}_{d_h}^i$. Building on the work of Cuchiero et al. [22], Cirone et al. [18, Theorem B.13] showed that choosing the A_θ^i to be dense Gaussian matrices with independent entries achieves maximal probabilistic expressivity. Unfortunately, using dense matrices is infeasible in practice due to computational constraints, as discussed in Section 2.2.

4 Structured linear controlled differential equations

4.1 Introduction

Building on Cirone et al. [18], we introduce Structured Linear Controlled Differential Equations (SLiCEs), a unifying framework for various choices of structured A_θ^i . This section presents three examples based on current models in the literature, diagonal, DPLR, and block-diagonal matrices, as well as two novel examples based on sparse matrices and the Walsh–Hadamard transform.

Our main theoretical results are Theorems 4.1, 4.2, and 4.3, which show that SLiCEs with block-diagonal, sparse, and Walsh–Hadamard matrices have maximal probabilistic expressivity. Formal proofs are given in Appendix A. These results complement [18, Theorem 4.3], which shows that SLiCEs with diagonal matrices are not maximally expressive and [65, Proposition D.2], which shows that SLiCEs with DPLR matrices have maximal probabilistic expressivity.

4.2 Diagonal-plus-low-rank LNCDEs

SSMs with diagonal state-transition matrices, such as S4 [35] and Mamba [34], are LNCDEs with diagonal matrices, $A_\theta^i = D_\theta^i$. Hence, they are not maximally expressive and underperform on state-tracking benchmarks [18, 59]. This limited expressivity motivates the use of alternative structured state-transition matrices.

DeltaNet, DeltaProduct, and Gated DeltaNet use specific versions of DPLR state-transition matrices [77, 93, 80, 94]. The general form of a DPLR-LNCDE is

$$A_\theta^i = D_\theta^i + \sum_{i=1}^r u_\theta^i (v_\theta^i)^\top, \quad (10)$$

where r is the rank. This parameterisation reduces the number of trainable parameters and computational cost of calculating a hidden state update from $\mathcal{O}(d_\omega d_h^2)$ to $\mathcal{O}(d_\omega r d_h)$. Furthermore, [65, Proposition D.2] shows that if $r \rightarrow \infty$ as $d_h \rightarrow \infty$, then DPLR-LNCDEs have maximal probabilistic expressivity.

4.3 Block-Diagonal LNCDEs

Block-diagonal state-transition matrices were first explored in LRNNs to improve performance on regular-language tasks [28]. Block-diagonal LNCDEs (BD-LNCDEs) use the same structure, but make the dependence on the input path linear,

$$A_\theta^i = \text{BlockDiag}(B_{\theta,1}^i, B_{\theta,2}^i, \dots, B_{\theta,k}^i), \quad (11)$$

where each $B_{\theta,j}^i \in \mathbb{R}^{b_j \times b_j}$ is a trainable dense block, k is the number of blocks, and b_j are the block-sizes, with $d_h = \sum_{j=1}^k b_j$. This parameterisation reduces the number of trainable parameters and computational cost of calculating a hidden state-update from $\mathcal{O}(d_\omega d_h^2)$ to $\mathcal{O}(d_\omega \sum_{j=1}^k b_j^2)$, providing a substantial speed-up when each $b_j \ll d_h$. Furthermore, this does not restrict the expressivity.

Theorem 4.1. *If $\max_j b_j \rightarrow \infty$ as $d_h \rightarrow \infty$, then block-diagonal LNCDEs have maximal probabilistic expressivity.*

Hence, the non-linear dependence of the input-dependent block-diagonal LRNN is not necessary for expressivity. Because the hidden state factorises into k independent parts, BD-LNCDEs can be viewed as a multi-head dense LNCDE (DE-LNCDE) of head sizes b_j . For a fixed d_h , choosing smaller blocks yields greater speed; choosing larger blocks yields greater expressivity. Under a fixed compute budget, there is a trade-off between expressivity and hidden dimension, and this is explored empirically in Appendix D.2.

4.4 Sparse LNCDEs

Let $0 < \epsilon < 1$. A sparse LNCDE (S-LNCDE) takes each A_θ^i to be a sparse matrix with $\mathcal{O}(d_h^{1+\epsilon})$ non-zero entries, selected at random according to a Bernoulli distribution. This reduces the parameter count and computational cost of calculating a hidden state update from $\mathcal{O}(d_\omega d_h^2)$ to $\mathcal{O}(d_\omega d_h^{1+\epsilon})$. Furthermore, it does not restrict the expressivity.

Theorem 4.2. *Sparse LNCDEs have maximal probabilistic expressivity.*

In theory, S-LNCDEs have faster training and inference times than DE-LNCDEs. In practice, current deep-learning frameworks (e.g. JAX [10], PyTorch [68]) are not optimised for unstructured sparsity, so practical speed-ups are not observed in our implementations. Nonetheless, we anticipate that ongoing work on sparse matrices will enable future gains in efficiency.

4.5 Walsh–Hadamard LNCDEs

A Hadamard matrix of order n is an $n \times n$ matrix H_n with entries ± 1 whose rows (and columns) are mutually orthogonal, $H_n H_n^\top = nI_n$, where I_n is the $n \times n$ identity matrix. When $n = 2^m$ for $m \in \mathbb{N}$, we can construct these matrices iteratively using the Sylvester construction [86]. Commonly, these matrices are applied via the Walsh–Hadamard transform (WHT), which admits an $\mathcal{O}(n \log n)$ algorithm [78]. Many scientific computing libraries include efficient CPU and GPU kernels for performing the Walsh–Hadamard transform [90, 1]. In practice, a normalisation factor of $n^{-1/2}$ can be applied to ensure the matrix is orthonormal [88].

Walsh–Hadamard LNCDEs replace each dense matrix A_θ^i by the product

$$A_\theta^i = HD_\theta^i, \quad (12)$$

where H is a normalised Hadamard matrix, and D_θ^i is a diagonal matrix. This parameterisation reduces the number of trainable parameters from $\mathcal{O}(d_\omega d_h^2)$ to $\mathcal{O}(d_\omega d_h)$. The cost of computing the hidden state update depends on the order of operations. If you first sum the diagonal matrices over the channels and then apply the fast Walsh–Hadamard transform, as is done in the RHS of (4), the cost is $\mathcal{O}(\max(d_\omega d_h, d_h \log(d_h)))$. This is substantially cheaper than the $\mathcal{O}(d_\omega d_h^2)$ for dense LNCDEs. Furthermore, this modification does not restrict the expressivity.

Theorem 4.3. *Walsh–Hadamard LNCDEs have maximal probabilistic expressivity.*

Model	Parameters	Recurrent Cost	Parallel Cost	Efficient Impl.	Maximally Expressive
DE-LNCDEs	$\mathcal{O}(d_h^3)$	$\mathcal{O}(nd_h^3)$	$\mathcal{O}(\log(n), d_h^3)$	Yes	Yes
D-LNCDEs	$\mathcal{O}(d_h^2)$	$\mathcal{O}(nd_h^2)$	$\mathcal{O}(\log(n), d_h^2)$	Yes	No
DPLR-LNCDEs	$\mathcal{O}(rd_h^2)$	$\mathcal{O}(nd_h^2)$	$\mathcal{O}(\log(n), d_h^3)$	Yes	Yes
S-LNCDEs	$\mathcal{O}(d_h^{2+\epsilon})$	$\mathcal{O}(nd_h^{2+\epsilon})$	$\mathcal{O}(\log(n), d_h^3)$	No	Yes
WH-LNCDEs	$\mathcal{O}(d_h^2)$	$\mathcal{O}(nd_h^2)$	$\mathcal{O}(\log(n), d_h^3)$	Yes	Yes
BD-LNCDEs	$\mathcal{O}\left(d_h \sum_j b_j^2\right)$	$\mathcal{O}\left(nd_h \sum_j b_j^2\right)$	$\mathcal{O}\left(\log(n), d_h \sum_j b_j^2\right)$	Yes	Yes

Table 1: Comparison of dense LNCDEs (DE-LNCDEs), diagonal LNCDEs (D-LNCDEs), diagonal-plus-low-rank LNCDEs (DPLR-LNCDEs), sparse LNCDEs (S-LNCDEs), Walsh–Hadamard LNCDEs (WH-LNCDEs), and block-diagonal LNCDEs (BD-LNCDEs) on parameter count, computational cost, the existence of an efficient implementation, and expressivity. Here, d_h is the hidden dimension, n is the sequence length, b_j are BD-LNCDE’s block-sizes, r is DPLR-LNCDE’s rank, ϵ is S-LNCDE’s sparsity, and for simplicity we have taken $d_\omega = d_h$. Parallel cost is measured as $\mathcal{O}(\text{scan depth, cost per composition})$ when applying a parallel associative scan.

4.6 Parallel computation

The recurrent cost of a SLiCE is based solely on the cost of calculating a single hidden state update, whereas the calculation when using an associative scan is repeatedly composing

$$\exp\left(\sum_{i=1}^{d_\omega} (\omega_{t_{j+1}}^i - \omega_{t_j}^i) A_\theta^i\right) \approx I + \sum_{i=1}^{d_\omega} (\omega_{t_{j+1}}^i - \omega_{t_j}^i) A_\theta^i, \quad (13)$$

where the first-order approximation of the exponential is often used in practice. When the A_θ^i are diagonal or block-diagonal, the composition of (13) preserves the structure, as these classes of matrices are closed under multiplication. Therefore, using a parallel associative scan reduces the scan depth from n to $\log(n)$, whilst having a computational cost per composition of $\mathcal{O}(d_h)$ or $\mathcal{O}(\sum_j b_j^3)$, respectively. However, for DPLR, sparse, and Walsh–Hadamard LNCDEs, the structured matrices are not closed under multiplication, which means that the limiting computational cost per composition is the same as a dense LNCDE, $\mathcal{O}(d_h^3)$. Table 1 summarises the differences in parameter count, computational cost, existence of an efficient implementation, and expressivity of all the SLiCEs considered in this paper, where for simplicity we have taken $d_\omega = d_h$.

For large models, parallel associative scans result in high I/O costs, as each state-transition matrix must be materialised in GPU memory [93]. A possible approach to mitigating I/O costs for SLiCEs is combining LNCDEs with the Log-ODE method. By approximating the solution over intervals, this method avoids explicitly materialising intermediate state-transition matrices. However, it does require computing the log-signature of the input path and iterated Lie brackets of the vector fields [91]. A detailed description of this approach is given in Appendix B. In Section 5.3, we implement a hybrid strategy: the Log-ODE method is applied to small intervals, and the resulting outputs are then processed using a parallel associative scan. Yang et al. [93] introduced an alternative approach for DeltaNet, where a chunk-wise algorithm specifically tailored for diagonal-plus-rank-one state-transition matrices is used to bypass the need to materialise every intermediate matrix, significantly cutting down I/O costs [93]. DeltaProduct extends this approach to handle DPLR matrices [80]. These approaches can also be applied to diagonal state-transition matrices. Therefore, a block-diagonal LNCDE with a large diagonal portion ($b_i = 1$ for $i = 1, \dots, k-1$) followed by a small dense block emerges as an attractive solution. The large diagonal section can efficiently utilise the chunk-wise algorithm and the smaller dense section can be processed using parallel associative scans without incurring significant I/O costs. Models of this type are explored empirically in Section 5.2.

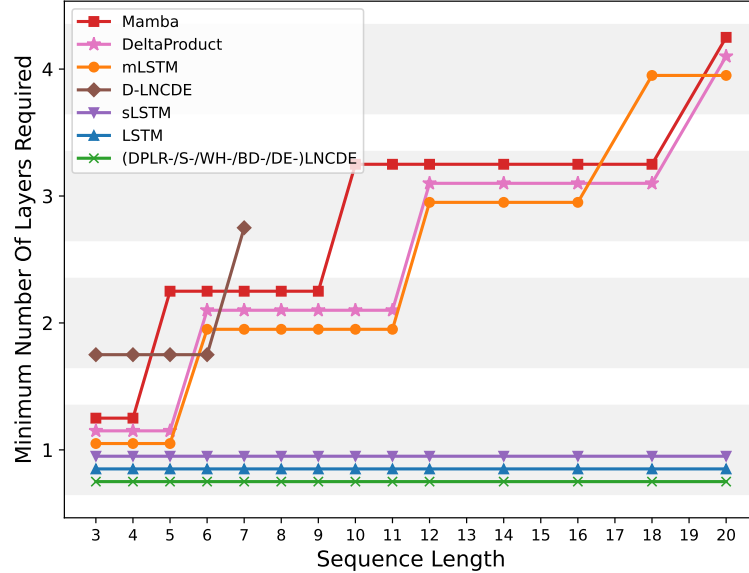


Figure 1: Results for Mamba, LSTM, mLSTM, sLSTM, Gated DeltaProduct with negative eigenvalues, dense LNCDE (DE-LNCDE), diagonal LNCDE (D-LNCDE), DPLR-LNCDE, sparse LNCDE (S-LNCDE), Walsh–Hadamard LNCDE (WH-LNCDE), and a fixed block-size block-diagonal LNCDE (BD-LNCDE) on the A_5 Benchmark. For each sequence length, the plot shows the minimum number of stacked layers each model requires to achieve greater than 90% validation accuracy. Each grey region indicates an equivalent number of stacked layers. Missing values indicate the model did not achieve greater than 90% validation accuracy with 4 or fewer stacked layers.

5 Experiments

5.1 The A_5 benchmark

The A_5 benchmark tests models on their ability to state-track [59]. Each sequence in the dataset consists of a series of permutations from the group of even permutations on five elements, denoted A_5 . The task is to compose the permutations, which requires state-tracking. We train and evaluate models on sequences ranging from length 3 to 20 and determine how many stacked layers each model needs to achieve a validation accuracy greater than 90%.

This benchmark serves as an empirical validation of our theoretical results; diagonal LNCDEs are less expressive than dense, DPLR, sparse, Walsh–Hadamard, and block-diagonal LNCDEs. In addition to the LNCDE models, we consider Mamba [34], LSTM [39], gated DeltaProduct with negative eigenvalues [94, 80], and the two components of xLSTM [6] (mLSTM and sLSTM) on this benchmark. All baselines use a hidden dimension of 1024 and all SLiCEs use 1024 parameters per state-transition matrix. Full experimental details are given in Appendix D.1.

Figure 1 shows that the diagonal state-transition matrices of Mamba, mLSTM, and diagonal LNCDE mean that an increasing number of stacked layers are needed as the sequence length grows. Interestingly, Gated DeltaProduct with negative eigenvalues, which uses a DPLR structure with $r = 2$, also needs a growing number of stacked layers. However, a DPLR-LNCDE with $r = 2$ only needs one layer for all sequence lengths, suggesting this is not an inherent limitation of DPLR state-transition matrices. Similarly, sparse, Walsh–Hadamard, block-diagonal, and dense LNCDEs, as well as the two recurrent baselines LSTM and sLSTM, all need only one layer for all sequence lengths.

5.2 Regular language tasks

The formal language benchmark is a collection of language style tasks split into categories using the Chomsky Hierarchy [27]. Here, we use the regular tasks, which can be solved by processing inputs sequentially with a fixed set of internal states and no external memory, i.e. state-tracking. On this

Table 2: Average and standard deviation of validation accuracy over five runs for a range of recurrent and parallel models on the formal language tasks.

Model	Cycle Nav.	Even Pairs	Mod Arith. No Brack.	Parity	Average
Recurrent					
LSTM	100.0 ± 0.0	100.0 ± 0.0	99.9 ± 0.1	100.0 ± 0.0	100
sLSTM	39.2 ± 4.3	100.0 ± 0.0	34.8 ± 1.5	100.0 ± 0.0	68.5
xLSTM[1:1]	56.6 ± 3.6	100.0 ± 0.0	34.4 ± 1.4	100.0 ± 0.0	72.8
Parallel					
DeltaNet	49.0 ± 5.4	100.0 ± 0.0	44.2 ± 8.0	58.4 ± 1.1	62.9
DeltaNet[−1, 1]	47.3 ± 6.0	100.0 ± 0.0	63.9 ± 7.2	97.2 ± 1.7	77.1
Gated DeltaNet	55.9 ± 7.8	100.0 ± 0.0	49.9 ± 7.5	56.6 ± 0.7	65.6
Gated DeltaProduct[−1,1]	61.4 ± 12.0	99.6 ± 0.6	58.0 ± 20.0	98.8 ± 1.5	79.5
RWKV-7	37.8 ± 5.0	88.1 ± 14.2	41.6 ± 13.8	51.0 ± 0.3	54.6
mLSTM	87.4 ± 4.5	100.0 ± 0.0	29.0 ± 5.1	50.9 ± 0.3	66.8
Transformer	24.4 ± 0.5	90.4 ± 10.4	23.6 ± 0.7	52.2 ± 0.4	47.7
Mamba	50.7 ± 7.8	100.0 ± 0.0	38.1 ± 6.0	54.5 ± 1.5	60.8
D-LNCDE	73.5 ± 4.7	100.0 ± 0.0	20.8 ± 0.3	91.9 ± 14.5	71.6
WH-LNCDE	66.7 ± 7.9	87.5 ± 17.2	23.9 ± 1.3	62.1 ± 2.2	60.1
BD ₄ -LNCDE	100.0 ± 0.0	91.3 ± 12.2	45.6 ± 7.8	88.4 ± 13.9	81.3
D-DE ₁₆ -LNCDE	77.3 ± 21.3	81.4 ± 9.9	94.5 ± 5.2	81.0 ± 18.1	83.6
DPLR ₄ -LNCDE	83.9 ± 20.1	97.7 ± 5.2	26.0 ± 0.7	79.6 ± 20.3	71.8
Random	20.0	50.0	20.0	50.0	35.0

benchmark, the models are challenged to generalise to longer sequences, by training on sequences from length 3 to 40 and evaluating on sequences from length 40 to 256. Details on the individual tasks can be found in Appendix D.2. A wide range of existing sequence model architectures are considered, including LSTM [39], xLSTM and its two components mLSTM and sLSTM [6], four variations of DeltaNet [77, 92, 94, 80, 33], RWKV-7 [69], a Transformer [89], and Mamba [34]. All models use two stacked layers. All models except Mamba use a hidden dimension of 128 or 512, with the choice determined by which yields higher validation accuracy on each dataset. Mamba uses a hidden dimension of 256 or 512, as it does not support a hidden size of 128. We consider five SLiCE variants: diagonal, DPLR_r (where r denotes the rank), Walsh–Hadamard, and two block-diagonal structures. The first uses a fixed block-size $b_i = b$ (denoted BD_b-LNCDE), while the second is a diagonal-dense LNCDE (D-DE_b-LNCDE), with $b_i = 1$ for $i = 1, \dots, k-1$ and $b_k = b > 1$. All SLiCEs use two stacked layers and 512 non-zero parameters per state-transition matrix, except for the diagonal and Walsh–Hadamard, which also consider 128, with the better performing choice reported for each dataset. For the DPLR, block-diagonal, and diagonal-dense LNCDEs, we consider multiple choices of rank and block-size, respectively, and present the best performing models. A thorough investigation of the effect of block-size and rank is given in Appendix D.2. We do not consider sparse LNCDE on this benchmark, due to the lack of an efficient implementation.

Table 2 presents the results. As expected, the recurrent LSTM generalises near perfectly on all four tasks. Amongst the parallel models, DeltaNet with negative eigenvalues and Gated DeltaProduct with negative eigenvalues are the best performing baselines, aligning with the expectation that increased complexity in the state-transition matrix improves state-tracking performance. Similarly, diagonal LNCDE outperforms Mamba, aligning with the results of Grazzi et al. [33] that expanding the eigenvalue range of the state-transition matrix improves state-tracking performance. Notably, the two block-diagonal SLiCE variants achieve the highest average validation accuracy among parallelisable models.

5.3 UEA multivariate time-series classification archive

Since SLiCEs are descendants of NCDEs, they inherit a number of the desirable properties which arise from having a natural continuous time formulation. These include robustness to irregular sampling rates and decoupling the number of recurrent steps from the number of observations in the time-series [48, 91]. Furthermore, SLiCEs have the same theoretical expressivity as NCDEs, whilst being parallel-in-time, making them an attractive alternative for real-world time-series modelling.

Table 3: Comparison of accuracy, average run-time, and average GPU memory for S6, Log-NCDE, diagonal LNCDE (D-LNCDE), block-diagonal LNCDE (BD-LNCDE), and dense LNCDE (DE-LNCDE) on six datasets from the UEA-MTSCA. Results marked with a * are from [91].

Dataset	S6*	Log-NCDE*	D-LNCDE	BD-LNCDE	DE-LNCDE
EigenWorms	85.0 ± 16.1	85.6 ± 5.1	80.0 ± 5.4	86.7 ± 4.1	87.8 ± 5.7
EthanolConcentration	26.4 ± 6.4	34.4 ± 6.4	25.8 ± 3.9	28.6 ± 6.4	25.6 ± 3.7
Heartbeat	76.5 ± 8.3	75.2 ± 4.6	72.9 ± 5.0	75.2 ± 6.0	76.1 ± 3.1
MotorImagery	51.3 ± 4.7	53.7 ± 5.3	54.0 ± 7.3	58.2 ± 4.1	54.0 ± 5.3
SelfRegulationSCP1	82.8 ± 2.7	83.1 ± 2.8	83.5 ± 2.1	84.9 ± 1.9	83.5 ± 6.6
SelfRegulationSCP2	49.9 ± 9.5	53.7 ± 4.1	53.0 ± 5.8	53.3 ± 7.5	46.3 ± 3.6
Average Accuracy	62.0	<u>64.3</u>	61.5	64.5	62.2
Average Rank	3.7	<u>2.8</u>	3.7	1.9	3.0
Average GPU memory (MB)	2608	1999	2159	2938	6723
Average Time / 1k steps (s)	20	1131	7	55	87

As a demonstration of the practical benefits, we consider six datasets from the UEA Multivariate Time-Series Classification Archive (UEA-MTSCA), a collection of time-series classification tasks, ranging from classifying worms into species based on movement to classifying alcohol by concentration using vibrational spectroscopy [4]. Walker et al. [91] showed that Log-NCDEs outperform the linear recurrent unit [66], S5 [81], S6 [34], and Mamba [34] on average test accuracy over the six longest datasets with at least 200 observations [91]. However, the per-step training time is much longer for Log-NCDEs than the baseline methods.

Keeping all other hyperparameters the same and using the same hardware (an NVIDIA RTX 4090), Table 3 shows the impact of replacing the non-linear vector field of a Log-NCDE with a diagonal, block-diagonal, and dense linear vector field. S6 is included as the best performing baseline from Walker et al. [91], with a comparison to all baseline models provided in Appendix D.3. Both the diagonal and dense linear vector fields lead to a drop in average test accuracy. Possible causes are the reduced expressivity of the diagonal linear vector fields and the large number of parameters in the dense linear vector fields leading to over-fitting. In contrast, block-diagonal LNCDE maintains the average test accuracy of Log-NCDE whilst reducing the average per-step training time by a factor of 20 and increasing the average GPU memory usage by only 50%.

6 Conclusion

This paper introduced SLiCEs, a unifying framework for sequence-to-sequence layers that are maximally expressive, computationally efficient, and allow for parallel-in-time computation. We explored four specific instances, DPLR, sparse, Walsh–Hadamard, and block-diagonal, analysing their theoretical properties and empirical performance. Theorems 4.1, 4.2, and 4.3 established that block-diagonal, sparse, and Walsh–Hadamard SLiCEs achieve maximal probabilistic expressivity. Furthermore, all SLiCE variants demonstrated state-tracking on the A_5 benchmark, unlike the other parallelisable layers considered: diagonal LNCDEs, mLSTM, Mamba, and DeltaProduct. Among the SLiCEs, block-diagonal LNCDE stands out as the only maximally expressive variant that strictly reduces parameter count, recurrent cost, and parallel cost compared to dense LNCDEs. Additionally, two block-diagonal LNCDE variants achieved the highest average validation accuracies among parallel models on the regular language tasks from the formal language benchmark. Finally, the practical speed-ups which can be achieved were demonstrated on six multivariate time-series classification datasets, where replacing the non-linear vector field of a Log-NCDE with a block-diagonal linear vector field reduced the average time per training step by a factor of twenty, without impacting the average test accuracy.

There are a number of avenues for potential future work. Alternative SLiCE architectures beyond those explored in this paper may achieve maximal expressivity and improved empirical performance. A theoretical characterisation of the conditions that a structured matrix needs to satisfy so that a SLiCE achieves maximal probabilistic expressivity would aid the search for additional structures. Additionally, although establishing maximal probabilistic expressivity is a significant step toward a deeper theoretical understanding of structured state-transition matrices, expressivity at finite hidden dimensions remains an open challenge.

Acknowledgements

We thank Joël Mouterde, Jérôme Tomezyk, Sam Morley, and Alexandre Bloch for engaging and insightful discussions on the design and training of linear neural controlled differential equations.

Terry Lyons was funded in part by the EPSRC [EP/S026347/1], in part by The Alan Turing Institute [EP/N510129/1], in part by the Defence and Security Programme, in part by the Office for National Statistics, and in part by the Hong Kong Innovation and Technology Commission (InnoHK Project CIMDA). Benjamin Walker was funded by the Hong Kong Innovation and Technology Commission (InnoHK Project CIMDA). Lingyi Yang is supported by EPSRC [EP/S026347/1] and the Hong Kong Innovation and Technology Commission (InnoHK Project CIMDA). Nicola Muca Cirone is supported by the EPSRC Centre for Doctoral Training in Mathematics of Random Systems: Analysis, Modelling and Simulation [EP/S023925/1]. The authors would like to acknowledge the use of the University of Oxford Advanced Research Computing (ARC) facility in carrying out this work.
<http://dx.doi.org/10.5281/zenodo.22558>

References

- [1] Krish Agarwal, Rishi Astra, Adnan Hoque, Mudhakar Srivatsa, Raghu Ganti, Less Wright, and Sijia Chen. Hadacore: Tensor core accelerated hadamard transform kernel. *arXiv preprint arXiv:2412.08832*, 2024.
- [2] Imanol Perez Arribas, Cristopher Salvi, and Lukasz Szpruch. Sig-sdes model for quantitative finance. In *ACM International Conference on AI in Finance*, 2020.
- [3] Jimmy Lei Ba, Jamie Ryan Kiros, and Geoffrey E Hinton. Layer normalization. *arXiv preprint arXiv:1607.06450*, 2016.
- [4] Anthony Bagnall, Hoang Anh Dau, Jason Lines, Michael Flynn, James Large, Aaron Bostrom, Paul Southam, and Eamonn Keogh. The uea multivariate time series classification archive, 2018, 2018. URL <https://arxiv.org/abs/1811.00075>.
- [5] Barbora Barancikova, Zhuoyue Huang, and Cristopher Salvi. Sigdiffusions: Score-based diffusion models for long time series via log-signature embeddings. *arXiv preprint arXiv:2406.10354*, 2024.
- [6] Maximilian Beck, Korbinian Pöppel, Markus Spanring, Andreas Auer, Oleksandra Prudnikova, Michael Kopp, Günter Klambauer, Johannes Brandstetter, and Sepp Hochreiter. xlstm: Extended long short-term memory. *arXiv preprint arXiv:2405.04517*, 2024.
- [7] Ali Behrouz, Peilin Zhong, and Vahab Mirrokni. Titans: Learning to memorize at test time, 2024. URL <https://arxiv.org/abs/2501.00663>.
- [8] Guy E. Blelloch. Prefix sums and their applications. (CMU-CS-90-190), 1990.
- [9] Horatio Boedihardjo, Xi Geng, Terry Lyons, and Danyu Yang. The signature of a rough path: Uniqueness. *Advances in Mathematics*, 293:720–737, 2016. ISSN 0001-8708.
- [10] James Bradbury, Roy Frostig, Peter Hawkins, Matthew James Johnson, Chris Leary, Dougal Maclaurin, George Necula, Adam Paszke, Jake VanderPlas, Skye Wanderman-Milne, and Qiao Zhang. JAX: composable transformations of Python+NumPy programs, 2018. URL <http://github.com/google/jax>.
- [11] Thomas Cass and Cristopher Salvi. Lecture notes on rough paths and applications to machine learning. *arXiv preprint arXiv:2404.06583*, 2024.
- [12] Fabienne Castell and Jessica Gaines. An efficient approximation method for stochastic differential equations by means of the exponential lie series. *Mathematics and Computers in Simulation*, 38(1):13–19, 1995. ISSN 0378-4754. doi: [https://doi.org/10.1016/0378-4754\(93\)E0062-A](https://doi.org/10.1016/0378-4754(93)E0062-A).
- [13] Kuo-Tsai Chen. Integration of paths, geometric invariants and a generalized baker-hausdorff formula. *Annals of Mathematics*, pages 163–178, 1957.
- [14] Rewon Child, Scott Gray, Alec Radford, and Ilya Sutskever. Generating long sequences with sparse transformers. *ArXiv*, abs/1904.10509, 2019. URL <https://api.semanticscholar.org/CorpusID:129945531>.
- [15] Nicola Muca Cirone and Cristopher Salvi. Rough kernel hedging. *arXiv preprint arXiv:2501.09683*, 2025.
- [16] Nicola Muca Cirone, Maud Lemercier, and Cristopher Salvi. Neural signature kernels as infinite-width-depth-limits of controlled resnets. *arXiv preprint arXiv:2303.17671*, 2023.
- [17] Nicola Muca Cirone, Jad Hamdan, and Cristopher Salvi. Graph expansions of deep neural networks and their universal scaling limits, 2024. URL <https://arxiv.org/abs/2407.08459>.
- [18] Nicola Muca Cirone, Antonio Orvieto, Benjamin Walker, Cristopher Salvi, and Terry Lyons. Theoretical foundations of deep selective state-space models. *Advances in Neural Information Processing Systems*, 2024.

[19] Thomas Cochrane, Peter Foster, Varun Chhabra, Maud Lemercier, Terry Lyons, and Christopher Salvi. Sk-tree: a systematic malware detection algorithm on streaming trees via the signature kernel. In *2021 IEEE International Conference on Cyber Security and Resilience (CSR)*, pages 35–40. IEEE, 2021.

[20] Samuel N. Cohen, Silvia Lui, Will Malpass, Giulia Mantoan, Lars Nesheim, Áureo de Paula, Andrew Reeves, Craig Scott, Emma Small, and Lingyi Yang. Nowcasting with signature methods. *arXiv:2305.10256*, 2023.

[21] Samuel N Cohen, James Foster, Peter Foster, Hang Lou, Terry Lyons, Sam Morley, James Morrill, Hao Ni, Edward Palmer, Bo Wang, Yue Wu, Lingyi Yang, and Weixin Yang. Subtle variations in sepsis-III definitions markedly affect predictive performance. *Nature Scientific Reports*, 2024.

[22] Christa Cuchiero, Lukas Gonon, Lyudmila Grigoryeva, Juan-Pablo Ortega, and Josef Teichmann. Expressive power of randomized signature. In *The Symbiosis of Deep Learning and Differential Equations*, 2021.

[23] George Cybenko. Approximation by superpositions of a sigmoidal function. *Mathematics of Control, Signals and Systems*, 2(4):303–314, 1989.

[24] Tri Dao and Albert Gu. Transformers are ssms: generalized models and efficient algorithms through structured state space duality. In *Proceedings of the 41st International Conference on Machine Learning*, ICML’24. JMLR.org, 2024.

[25] Tri Dao, Beidi Chen, Nimit Sharad Sohoni, Arjun D Desai, Michael Poli, Jessica Grogan, Alexander Liu, Aniruddh Rao, Atri Rudra, and Christopher Ré. Monarch: Expressive structured matrices for efficient and accurate training. In *International Conference on Machine Learning*, 2022. URL <https://api.semanticscholar.org/CorpusID:247922732>.

[26] Yann N Dauphin, Angela Fan, Michael Auli, and David Grangier. Language modeling with gated convolutional networks. In *Proceedings of the 34th International Conference on Machine Learning*, pages 933–941. PMLR, 2017.

[27] Grégoire Delétang, Anian Ruoss, Jordi Grau-Moya, Tim Genewein, Li Kevin Wenliang, Elliot Catt, Chris Cundy, Marcus Hutter, Shane Legg, Joel Veness, and Pedro A. Ortega. Neural networks and the chomsky hierarchy. In *11th International Conference on Learning Representations*, 2023.

[28] Ting-Han Fan, Ta-Chung Chi, and Alexander Rudnicky. Advancing regular language reasoning in linear recurrent neural networks. In Kevin Duh, Helena Gomez, and Steven Bethard, editors, *Proceedings of the 2024 Conference of the North American Chapter of the Association for Computational Linguistics: Human Language Technologies (Volume 2: Short Papers)*, pages 45–53, Mexico City, Mexico, June 2024. Association for Computational Linguistics. doi: 10.18653/v1/2024.naacl-short.4. URL <https://aclanthology.org/2024.naacl-short.4/>.

[29] Adeline Fermanian, Terry Lyons, James Morrill, and Christopher Salvi. New directions in the applications of rough path theory. *IEEE BITS the Information Theory Magazine*, 2023.

[30] Jonathan Frankle and Michael Carbin. The lottery ticket hypothesis: Finding sparse, trainable neural networks. In *International Conference on Learning Representations*, 2019.

[31] Xavier Gonzalez, Andrew Warrington, Jimmy T. H. Smith, and Scott W. Linderman. Towards scalable and stable parallelization of nonlinear rnns. In *Advances in Neural Information Processing Systems (NeurIPS)*, 2024. URL <https://doi.org/10.48550/arXiv.2407.19115>.

[32] Benjamin Graham. Sparse arrays of signatures for online character recognition. 2013.

[33] Riccardo Grazzi, Julien Siems, Jörg K. H. Franke, Arber Zela, Frank Hutter, and Massimiliano Pontil. Unlocking state-tracking in linear rnns through negative eigenvalues, 2024. URL <https://arxiv.org/abs/2411.12537>.

[34] Albert Gu and Tri Dao. Mamba: Linear-time sequence modeling with selective state spaces. *arXiv:2312.00752*, 2023.

[35] Albert Gu, Karan Goel, and Christopher Ré. Efficiently modeling long sequences with structured state spaces. *arXiv preprint arXiv:2111.00396*, 2021.

[36] Marshall Hall. A basis for free lie rings and higher commutators in free groups. In *Proceedings of the American Mathematical Society*, volume 1, pages 575–581, 1950.

[37] B. Hambly and T. Lyons. Uniqueness for the signature of a path of bounded variation and the reduced path group. *Annals of Mathematics*, 171:109–167, 2010.

[38] Yihui He, Xiangyu Zhang, and Jian Sun. Channel pruning for accelerating very deep neural networks. In *The IEEE International Conference on Computer Vision (ICCV)*, Oct 2017.

[39] Sepp Hochreiter and Jürgen Schmidhuber. Long short-term memory. *Neural Comput.*, 9(8):1735–1780, nov 1997. ISSN 0899-7667. doi: 10.1162/neco.1997.9.8.1735. URL <https://doi.org/10.1162/neco.1997.9.8.1735>.

[40] Melker Hoglund, Emilio Ferrucci, Camilo Hernández, Aitor Muguruza Gonzalez, Christopher Salvi, Leandro Sanchez-Betancourt, and Yufei Zhang. A neural rde approach for continuous-time non-markovian stochastic control problems. *arXiv preprint arXiv:2306.14258*, 2023.

[41] Christian Holberg and Christopher Salvi. Exact gradients for stochastic spiking neural networks driven by rough signals. *arXiv preprint arXiv:2405.13587*, 2024.

[42] Kurt Hornik. Approximation capabilities of multilayer feedforward networks. *Neural Networks*, 4(2):251–257, 1991.

[43] Blanka Horvath, Maud Lemercier, Chong Liu, Terry Lyons, and Christopher Salvi. Optimal stopping via distribution regression: a higher rank signature approach. *arXiv preprint arXiv:2304.01479*, 2023.

[44] Zacharia Issa, Blanka Horvath, Maud Lemercier, and Christopher Salvi. Non-adversarial training of neural sdes with signature kernel scores. *Advances in Neural Information Processing Systems*, 36, 2024.

[45] Patrick Kidger. On neural differential equations. *arXiv:2202.02435*, 2022.

[46] Patrick Kidger. On neural differential equations, 2022. URL <https://arxiv.org/abs/2202.02435>.

[47] Patrick Kidger, Patric Bonnier, Imanol Perez Arribas, Christopher Salvi, and Terry Lyons. Deep signature transforms. In H. Wallach, H. Larochelle, A. Beygelzimer, F. d’Alché-Buc, E. Fox, and R. Garnett, editors, *Advances in Neural Information Processing Systems*, volume 32. Curran Associates, Inc., 2019. URL https://proceedings.neurips.cc/paper_files/paper/2019/file/d2cdf047a6674cef251d56544a3cf029-Paper.pdf.

[48] Patrick Kidger, James Morrill, James Foster, and Terry Lyons. Neural Controlled Differential Equations for Irregular Time Series. In *Advances in Neural Information Processing Systems*, 2020.

[49] Diederik P. Kingma and Jimmy Ba. Adam: A method for stochastic optimization. *arXiv:1412.6980*, 2017.

[50] Maud Lemercier, Christopher Salvi, Thomas Cass, Edwin V Bonilla, Theodoros Damoulas, and Terry Lyons. Siggpde: Scaling sparse gaussian processes on sequential data. In *International Conference on Machine Learning*. PMLR, 2021.

[51] Maud Lemercier, Christopher Salvi, Theodoros Damoulas, Edwin Bonilla, and Terry Lyons. Distribution regression for sequential data. In *International Conference on Artificial Intelligence and Statistics*, pages 3754–3762. PMLR, 2021.

[52] Daniel Levin, Terry Lyons, and Hao Ni. Learning from the past, predicting the statistics for the future, learning an evolving system, 2016. URL <https://arxiv.org/abs/1309.0260>.

[53] Yi Heng Lim, Qi Zhu, Joshua Selfridge, and Muhammad Firmansyah Kasim. Parallelizing non-linear sequential models over the sequence length, 2024.

[54] Bingbin Liu, Jordan T. Ash, Surbhi Goel, Akshay Krishnamurthy, and Cyril Zhang. Transformers learn shortcuts to automata. In *International Conference on Learning Representations*, 2023.

[55] T.J. Lyons, M. Caruana, and T. Lévy. *Differential Equations Driven by Rough Paths: École D'été de Probabilités de Saint-Flour XXXIV-2004*. Springer, 2007.

[56] Georg Manten, Cecilia Casolo, Emilio Ferrucci, Søren Wengel Mogensen, Christopher Salvi, and Niki Kilbertus. Signature kernel conditional independence tests in causal discovery for stochastic processes. *arXiv preprint arXiv:2402.18477*, 2024.

[57] Eric Martin and Chris Cundy. Parallelizing linear recurrent neural nets over sequence length. In *International Conference on Learning Representations*, 2018.

[58] William Merrill and Ashish Sabharwal. The parallelism tradeoff: Limitations of log-precision transformers. *Transactions of the Association for Computational Linguistics*, 2023.

[59] William Merrill, Jackson Petty, and Ashish Sabharwal. The illusion of state in state-space models. *arXiv preprint arXiv:2404.08819*, 2024.

[60] Asit K. Mishra, Jorge Albericio Latorre, Jeff Pool, Darko Stosic, Dusan Stosic, Ganesh Venkatesh, Chong Yu, and Paulius Micikevicius. Accelerating sparse deep neural networks. *ArXiv*, abs/2104.08378, 2021. URL <https://api.semanticscholar.org/CorpusID:233296249>.

[61] James Morrill, Andrey Kormilitzin, Alejo Nevado-Holgado, Sumanth Swaminathan, Sam Howison, and Terry Lyons. The signature-based model for early detection of sepsis from electronic health records in the intensive care unit. *2019 Computing in Cardiology (CinC)*, pages Page 1–Page 4, 2019.

[62] James Morrill, Christopher Salvi, Patrick Kidger, and James Foster. Neural rough differential equations for long time series. In *International Conference on Machine Learning*, pages 7829–7838. PMLR, 2021.

[63] James Morrill, Christopher Salvi, Patrick Kidger, James Foster, and Terry Lyons. Neural rough differential equations for long time series, 2021.

[64] James Morrill, Patrick Kidger, Lingyi Yang, and Terry Lyons. On the choice of interpolation scheme for neural CDEs. *Transactions of Machine Learning Research*, 2022.

[65] Sajad Movahedi, Felix Sarnthein, Nicola Muca Cirone, and Antonio Orvieto. Fixed-point rnns: From diagonal to dense in a few iterations, 2025. URL <https://arxiv.org/abs/2503.10799>.

[66] Antonio Orvieto, Samuel L Smith, Albert Gu, Anushan Fernando, Caglar Gulcehre, Razvan Pascanu, and Soham De. Resurrecting recurrent neural networks for long sequences. *arXiv:2303.06349*, 2023.

[67] Alexandre Pannier and Christopher Salvi. A path-dependent pde solver based on signature kernels. *arXiv preprint arXiv:2403.11738*, 2024.

[68] Adam Paszke, Sam Gross, Francisco Massa, Adam Lerer, James Bradbury, Gregory Chanan, Trevor Killeen, Zeming Lin, Natalia Gimelshein, Luca Antiga, Alban Desmaison, Andreas Köpf, Edward Yang, Zach DeVito, Martin Raison, Alykhan Tejani, Sasank Chilamkurthy, Benoit Steiner, Lu Fang, Junjie Bai, and Soumith Chintala. Pytorch: An imperative style, high-performance deep learning library, 2019. URL <https://arxiv.org/abs/1912.01703>.

[69] Bo Peng, Ruichong Zhang, Daniel Goldstein, Eric Alcaide, Xingjian Du, Haowen Hou, Jiaju Lin, Jiaxing Liu, Janna Lu, William Merrill, Guangyu Song, Kaifeng Tan, Saiteja Utpala, Nathan Wilce, Johan S. Wind, Tianyi Wu, Daniel Wuttke, and Christian Zhou-Zheng. Rwkv-7 "goose" with expressive dynamic state evolution, 2025. URL <https://arxiv.org/abs/2503.14456>.

[70] Hao Peng, Nikolaos Pappas, Dani Yogatama, Roy Schwartz, Noah A Smith, and Lingpeng Kong. Random feature attention. In *International Conference on Learning Representations (ICLR)*, 2021.

[71] Zhen Qin, Songlin Yang, Weixuan Sun, Xuyang Shen, Dong Li, Weigao Sun, and Yiran Zhong. Hgrn2: Gated linear rnns with state expansion, 2024.

[72] C. Reutenauer. *Free Lie Algebras*. LMS monographs. Clarendon Press, 1993.

[73] Cristopher Salvi. *Rough paths, kernels, differential equations and an algebra of functions on streams*. PhD thesis, University of Oxford, 2021.

[74] Cristopher Salvi, Thomas Cass, James Foster, Terry Lyons, and Weixin Yang. The signature kernel is the solution of a Goursat PDE. *SIAM Journal on Mathematics of Data Science*, 3(3):873–899, 2021.

[75] Cristopher Salvi, Maud Lemercier, Chong Liu, Blanka Horvath, Theodoros Damoulas, and Terry Lyons. Higher order kernel mean embeddings to capture filtrations of stochastic processes. *Advances in Neural Information Processing Systems*, 34:16635–16647, 2021.

[76] Cristopher Salvi, Joscha Diehl, Terry Lyons, Rosa Preiss, and Jeremy Reizenstein. A structure theorem for streamed information. *Journal of Algebra*, 634:911–938, 2023.

[77] Imanol Schlag, Kazuki Irie, and Jürgen Schmidhuber. Linear transformers are secretly fast weight programmers. In *Proceedings of the International Conference on Machine Learning (ICML)*, Proceedings of Machine Learning Research (PMLR), 2021. URL <https://proceedings.mlr.press/v139/schlag21a.html>.

[78] John L Shanks. Computation of the fast walsh-fourier transform. *IEEE Transactions on Computers*, 100(5):457–459, 1969.

[79] Daniil Shmelev and Cristopher Salvi. Sparse signature coefficient recovery via kernels. *arXiv preprint arXiv:2412.08579*, 2024.

[80] Julien Siems, Timur Carstensen, Arber Zela, Frank Hutter, Massimiliano Pontil, and Riccardo Grazzi. Deltaproduct: Improving state-tracking in linear rnns via householder products, 2025. URL <https://arxiv.org/abs/2502.10297>.

[81] Jimmy T. H. Smith, Andrew Warrington, and Scott W. Linderman. Simplified state space layers for sequence modeling. In *International Conference on Learning Representations*, 2023.

[82] Nitish Srivastava, Geoffrey Hinton, Alex Krizhevsky, Ilya Sutskever, and Ruslan Salakhutdinov. Dropout: A simple way to prevent neural networks from overfitting. *Journal of Machine Learning Research*, 15(56):1929–1958, 2014.

[83] M. H. Stone. The generalized weierstrass approximation theorem. *Mathematics Magazine*, 21(4):167–184, 1948. ISSN 0025570X, 19300980. URL <http://www.jstor.org/stable/3029750>.

[84] Nikko Ström. Sparse connection and pruning in large dynamic artificial neural networks. In *European Conference on Speech Communication and Technology (EUROSPEECH)*, 1997.

[85] Yu Sun, Xinhao Li, Karan Dalal, Jiarui Xu, Arjun Vikram, Genghan Zhang, Yann Dubois, Xinlei Chen, Xiaolong Wang, Sanmi Koyejo, Tatsunori Hashimoto, and Carlos Guestrin. Learning to (learn at test time): Rnns with expressive hidden states, 2025. URL <https://arxiv.org/abs/2407.04620>.

[86] James Joseph Sylvester. Thoughts on inverse orthogonal matrices, simultaneous signsuccessions, and tessellated pavements in two or more colours, with applications to newton’s rule, ornamental tile-work, and the theory of numbers. *The London, Edinburgh, and Dublin Philosophical Magazine and Journal of Science*, 34(232):461–475, 1867.

[87] Hidenori Tanaka, Daniel Kunin, Daniel L Yamins, and Surya Ganguli. Pruning neural networks without any data by iteratively conserving synaptic flow. In H. Larochelle, M. Ranzato, R. Hadsell, M.F. Balcan, and H. Lin, editors, *Advances in Neural Information Processing Systems*, volume 33, pages 6377–6389. Curran Associates, Inc., 2020. URL https://proceedings.neurips.cc/paper_files/paper/2020/file/46a4378f835dc8040c8057beb6a2da52-Paper.pdf.

[88] Giacomo Torlai, Christopher J Wood, Atithi Acharya, Giuseppe Carleo, Juan Carrasquilla, and Leandro Aolita. Quantum process tomography with unsupervised learning and tensor networks. *Nature Communications*, 14(1):2858, 2023.

[89] Ashish Vaswani, Noam Shazeer, Niki Parmar, Jakob Uszkoreit, Llion Jones, Aidan N Gomez, Łukasz Kaiser, and Illia Polosukhin. Attention is all you need. *Advances in neural information processing systems*, 30, 2017.

[90] Pauli Virtanen, Ralf Gommers, Travis E. Oliphant, Matt Haberland, Tyler Reddy, David Cournapeau, Evgeni Burovski, Pearu Peterson, Warren Weckesser, Jonathan Bright, Stéfan J. van der Walt, Matthew Brett, Joshua Wilson, K. Jarrod Millman, Nikolay Mayorov, Andrew R. J. Nelson, Eric Jones, Robert Kern, Eric Larson, C J Carey, İlhan Polat, Yu Feng, Eric W. Moore, Jake VanderPlas, Denis Laxalde, Josef Perktold, Robert Cimrman, Ian Henriksen, E. A. Quintero, Charles R. Harris, Anne M. Archibald, Antônio H. Ribeiro, Fabian Pedregosa, Paul van Mulbregt, and SciPy 1.0 Contributors. SciPy 1.0: Fundamental Algorithms for Scientific Computing in Python. *Nature Methods*, 17:261–272, 2020. doi: 10.1038/s41592-019-0686-2.

[91] Benjamin Walker, Andrew D. McLeod, Tiexin Qin, Yichuan Cheng, Haoliang Li, and Terry Lyons. Log neural controlled differential equations: The lie brackets make a difference. *International Conference on Machine Learning*, 2024.

[92] Songlin Yang, Bailin Wang, Yikang Shen, Rameswar Panda, and Yoon Kim. Gated linear attention transformers with hardware-efficient training, 2024. URL <https://arxiv.org/abs/2312.06635>.

[93] Songlin Yang, Bailin Wang, Yu Zhang, Yikang Shen, and Yoon Kim. Parallelizing linear transformers with the delta rule over sequence length. In *The Thirty-eighth Annual Conference on Neural Information Processing Systems*, 2024.

[94] Songlin Yang, Jan Kautz, and Ali Hatamizadeh. Gated delta networks: Improving mamba2 with delta rule, 2025. URL <https://arxiv.org/abs/2412.06464>.

[95] Yuxuan Zhang, Shiliang Yang, Rong Zhu, Yichong Zhang, Lei Cui, Yongjing Wang, Bin Wang, Feng Shi, Bing Wang, Wei Bi, Ping Zhou, and Guoxin Fu. Gated slot attention for efficient linear-time sequence modeling. In *Proceedings of the Thirty-eighth Annual Conference on Neural Information Processing Systems (NeurIPS)*, 2024.

A Expressivity

A.1 Introduction

Recall the core of our models is given by the controlled differential equation (1):

$$dh_s = \sum_{i=1}^{d_\omega} A^i h_s d\omega_s^i, \quad h_0 \in \mathbb{R}^{d_h}. \quad (14)$$

By [18, Proposition B.4], this can be written in terms of the *signature* as

$$\mathbf{h}((A^i)_i, h_0, \omega)_t := h_t = \sum_{I \in \mathbb{W}_{d_\omega}} (A^I h_0) S^I(\omega)_{[0,t]}, \quad (15)$$

where \mathbb{W}_{d_ω} is the set of words in the alphabet $[[d_\omega]] := \{1, \dots, d_\omega\}$ (i.e. $\mathbb{W}_{d_\omega} = \bigcup_{n \geq 0} [[d_\omega]]^n$) and for a given word $I = i_1 \dots i_n$ with $S^I(\omega)_{[0,t]}$ referring to the I th component of the signature tensor $S(\omega)_{[0,t]}$ i.e.

$$S^I(\omega)_{[0,t]} = \underbrace{\int \dots \int}_{\substack{u_1 < \dots < u_n \\ u_i \in [0,t]}} d\omega_{u_1}^{i_1} \dots d\omega_{u_n}^{i_n}.$$

By the classical Stone–Weierstrass theorem [83], linear functionals operating on signatures are dense in the space of continuous real-valued functions defined on compact sets of unparameterised paths [55, 37, 9]. This density property makes signature coefficients particularly well-suited as feature representations for machine learning tasks involving sequential data [52, 29, 11]. These techniques have experienced substantial growth in popularity and have been successfully implemented across diverse domains, with applications spanning deep learning [32, 47, 63, 64, 16, 40, 18, 91, 44, 5], kernel methods [74, 73, 51, 50, 56], and quantitative finance [2, 75, 43, 20, 67, 15]. Additionally, signature methods have proven valuable in information theory [76, 79], cybersecurity [19], sepsis detection [61, 21], and computational neuroscience [41], demonstrating their versatility across scientific disciplines.

It is evident from (15) that any linear readout of h_t is expressed as a series in signature terms. Consequently, such systems are inherently limited to learning functions that are close to these (uniformly convergent) series. *Maximal expressivity* is thus achieved when *any* finite linear combination in signature terms can be approximated by a linear readout on h_t through appropriate choices of the matrices A^i .

Definition A.1. Fix a set of paths $\mathcal{X} \subseteq C^{1-var}([0, 1]; \mathbb{R}^d)$. We say that a sequence $(\mathcal{A}_N, \mathcal{H}_N)_{N \in \mathbb{N}}$, where $\mathcal{H}_N \subseteq \mathbb{R}^N$ and $\mathcal{A}_N \subseteq \mathbb{R}^{N \times N}$, achieves *maximal expressivity* for \mathcal{X} whenever for any positive tolerance $\epsilon > 0$ and any finite linear combination coefficients $\alpha \in T(\mathbb{R}^d)$, there exist a choice of parameters $v, (A^i), h_0$ in some $\mathbb{R}^N, \mathcal{A}_N, \mathcal{H}_N$ in the sequence, such that $v^\top \mathbf{h}((A^i), h_0, \omega)_t$ is uniformly close to $\langle \alpha, S(\omega)_{[0,t]} \rangle$ up to an error of ϵ , i.e.

$$\begin{aligned} \forall \epsilon > 0, \forall \alpha \in T(\mathbb{R}^d), \exists N \geq 0, \exists (v, (A^i), h_0) \in \mathbb{R}^N \times \mathcal{A}_N^d \times \mathcal{H}_N \text{ s.t.} \\ \sup_{(\omega, t) \in \mathcal{X} \times [0, 1]} |\langle \alpha, S(\omega)_{[0,t]} \rangle - v^\top \mathbf{h}((A^i), h_0, \omega)_t| < \epsilon. \end{aligned}$$

If we are given a sequence of probabilities \mathbb{P}_N on $\mathcal{A}_N^d \times \mathcal{H}_N$ such that $\forall \epsilon > 0, \forall \alpha \in T(\mathbb{R}^d)$, it holds that

$$\lim_{N \rightarrow \infty} \mathbb{P}_N \left\{ \exists v \in \mathbb{R}^N \text{ s.t.} \sup_{(\omega, t) \in \mathcal{X} \times [0, 1]} |\langle \alpha, S(\omega)_{[0,t]} \rangle - v^\top \mathbf{h}((A^i), h_0, \omega)_t| < \epsilon \right\} = 1, \quad (16)$$

then we say that $(\mathcal{A}_N, \mathcal{H}_N, \mathbb{P}_N)_{N \in \mathbb{N}}$ achieves *maximal probabilistic expressivity* for \mathcal{X} .

A deterministic argument by [46] demonstrates the existence of a specific choice of $\mathcal{A}_N, \mathcal{H}_N$ that mimics the algebraic structure of tensors and provides *maximal expressivity* for compact sets of paths. Furthermore, Cirone et al. [18, Theorem B.13] established that matrices (almost) replicating the

algebraic structure of tensors are, in fact, abundant. They showed that the triplet $(\mathbb{R}^{N \times N}, \mathbb{R}^N, \mathbb{P}_N)$, where \mathbb{P}_N is a Gaussian measure achieves *maximal probabilistic expressivity* for compact sets.

The result in [18] implies that for dense matrices A^i , if the hidden dimension N is sufficiently large, there is a significant abundance of parameters capable of achieving uniformly and arbitrarily low error rates. These parameters should therefore be readily discoverable through classical optimisation methods. Unfortunately, as discussed in Section 2.2, using dense matrices is infeasible in practice due to computational constraints. In this section, we present three alternative choices of parameters that lead to *maximal probabilistic expressivity* for compact sets. These alternatives offer better computational properties compared to the naive use of dense matrices.

A.2 Sparse Matrices

Proposition A.2. *The sequence of triplets $(\mathbb{R}^{N \times N}, \mathbb{R}^N, \mathbb{P}_N)$ where \mathbb{P}_N is such that*

- *the initial value has independent standard Gaussian entries $[h_0]_\alpha \stackrel{\text{iid}}{\sim} \mathcal{N}(0, 1)$,*
- *the weight matrices are distributed as $A^i \stackrel{\text{iid}}{\sim} \frac{1}{\sqrt{N}p_N} W \odot B$ with W and B independent matrices having entries $[W]_{\alpha, \beta} \stackrel{\text{iid}}{\sim} \mathcal{N}(0, 1)$ and $[B]_{\alpha, \beta} \stackrel{\text{iid}}{\sim} \text{Ber}(p_N)$,*
- *the sparsity parameter p_N satisfies $Np_N \rightarrow \infty$ as $N \rightarrow \infty$,*

achieves maximal probabilistic expressivity for compact sets.

Proof. Following Cirone et al. [18, Section B.3.5], we only need to prove a bound of type

$$\left\| \frac{1}{N} \langle A_I h_0, A_J h_0 \rangle_{\mathbb{R}^N} - \delta_{I,J} \right\|_{L^2(\mathbb{P}_N)} \leq (\kappa(|I| + |J|))!! \mathcal{O}\left(\frac{1}{\sqrt{N}}\right) \quad (17)$$

as in the dense Gaussian case. That such sparse matrices present the same bounds as dense Gaussian ones follows from [17, Section 6.2], where it is shown that the bounds can only differ by a correction term of order $\mathcal{O}_{I,J}\left(\frac{1}{\sqrt{N}}\right)$ where the constants are bounded by the number of pairings of $I \cup J \cup I \cup J$. \square

Remark A.3. Following Cirone et al. [17, Section 6.1], it is possible to prove that W can be taken as having i.i.d. entries from a centred, symmetric but heavy tailed distribution given finiteness of even moments.

A.3 Walsh–Hadamard Matrices

Proposition A.4. *The sequence of triplets $(\mathcal{A}_N, \mathbb{R}^N, \mathbb{P}_N)$ where \mathcal{A}_N and \mathbb{P}_N are such that*

- $\mathcal{A}_N := \{W \text{diag}(\Delta) : \Delta \in \mathbb{R}^N, W \in \mathbb{R}^{N \times N}, WW^\top = I_N\},$
- *the initial value has independent standard Gaussian entries $[h_0]_\alpha \stackrel{\text{iid}}{\sim} \mathcal{N}(0, 1)$,*
- *the weight matrices are distributed as $A^i \stackrel{\text{iid}}{\sim} \frac{1}{\sqrt{N}} H \text{diag}(\Delta)$ for a fixed $H \in \mathbb{R}^{N \times N}$ satisfying $HH^\top = NI_N$ and having entries bounded uniformly in N by a constant C , and $\Delta \in \mathbb{R}^N$ having entries $[\Delta]_\alpha \stackrel{\text{iid}}{\sim} \mathcal{N}(0, 1)$,*

achieves maximal probabilistic expressivity for compact sets. In particular one can choose H to be a Walsh–Hadamard matrix of order N for computational efficiency.

Proof. Following Cirone et al. [18, Section B.3.5], we only need to prove a bound of type

$$\left\| \frac{1}{N} \langle A_I h_0, A_J h_0 \rangle_{\mathbb{R}^N} - \delta_{I,J} \right\|_{L^2(\mathbb{P}_N)} \leq (\kappa(|I| + |J|))!! \mathcal{O}\left(\frac{1}{\sqrt{N}}\right). \quad (18)$$

We will place ourselves in the graphical setting of [17] and leverage the fact that (c.f. [17, Section 7.1]) their results and techniques hold even when the vertices are fixed to random vectors.

The first step is to notice that for $x \in \mathbb{R}^N$ one has the equivalence $W\text{diag}(\Delta) \cdot x = W \cdot (\Delta \odot x)$ which can be represented graphically as in Figure 2.

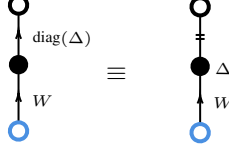


Figure 2: Graphical representations of the matrix $W\text{diag}(\Delta)$. Here \dagger edges correspond to identity matrices.

This leads to the *product graph* representation $G_{I,J}$ for $\frac{1}{N} \langle A_I h_0, A_J h_0 \rangle_{\mathbb{R}^N}$, where $I = i_1 \dots i_n$ and $J = j_1 \dots j_m$, given in Figure 3, which allow us to use [17, Proposition 1] to obtain the bounds.

$$\frac{1}{N} \langle A_I h_0, A_J h_0 \rangle \equiv \frac{1}{N} \frac{1}{N^{\frac{n+m}{2}}} h_0 \xrightarrow{H} \Delta_{i_n} \xrightarrow{H} \dots \xrightarrow{H} \Delta_{i_1} \xrightarrow{H} h_0 \quad \Delta_{j_1} \xrightarrow{H} \dots \xrightarrow{H} \Delta_{j_m} \xrightarrow{H} h_0$$

Figure 3: The product $\frac{1}{N} \langle A_I h_0, A_J h_0 \rangle_{\mathbb{R}^N}$ as a *product graph* G .

In the present setting, the vertices labelled h_0 must be identified, and the remaining decorated vertices must be paired such that Δ_a is identified with Δ_b only if $a = b$. Each of these *admissible pairings* ϕ produces a graph $(G_{I,J})_\phi$ in which each vertex is assigned the vector of ones. Note that since $|[H]_{\alpha,\beta}| \leq C$, one has $|H^{\odot k}| \leq C^k$. The procedure is shown in Figure 4 for all pairings when $I = J = 11$.

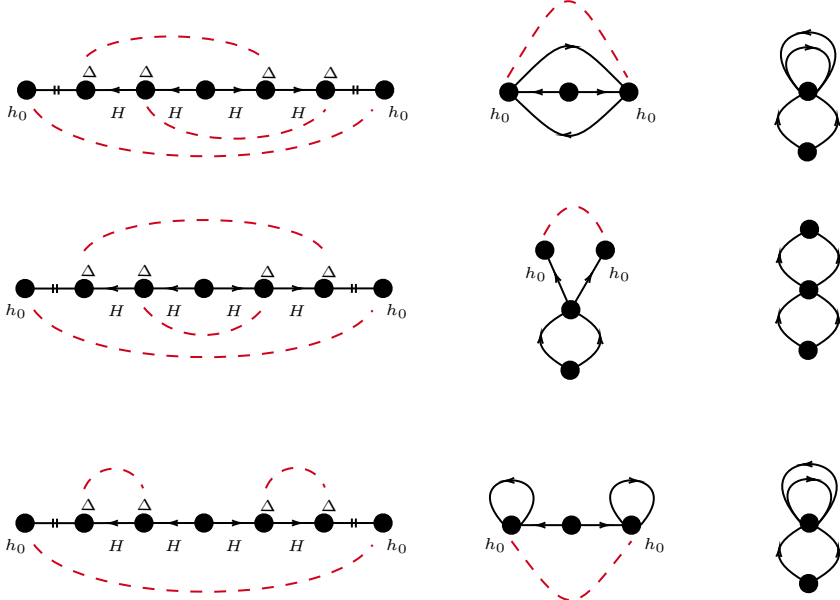


Figure 4: Construction of $(G_{I,J})_\phi$. Here, we display all the pairings, represented by the red dashed lines, for $I = J = 11$ along with their intermediate stages. For simplicity, we omit the H labels from edges with arrows.

Under these boundedness assumptions, note how leading-order pairings of $G_{I,J}$ are the ones having the maximum number of surviving vertices, meaning having $\frac{|I|+|J|}{2} + 1$ vertices. This can happen iff $I = J$, and even in this case, there exists only one pairing (the middle one in Figure 4) for which it holds that $(G_{I,J})_\phi \equiv \frac{1}{N} \frac{1}{N^{\frac{2|I|}{2}}} N^{|I|+1} = 1$. To see this, note that only the "middle" vertex of $G_{I,J}$ is

not paired, so to get $\frac{|I|+|J|}{2} + 1$, all other vertices have to be identified in couples. This implies that the left and right adjacent vertices (call them v_l and v_r) must be paired together: in fact the sub-graph comprising the middle vertex and the two adjacent edges corresponds to the matrix $HH^\top = NI_N$, hence we can remove this sub-graph, identify the adjacent vertices and take the factor N in front without changing the value of the graph; but then if v_l and v_r were paired with other vertices we would identify at least 4 vertices. Hence i_1 has to be equal to j_1 and v_l and v_r must be identified. Proceeding by induction, from the middle out, we see that only the identity pairing has non-vanishing value.

To conclude we are left to prove that any pairing ψ of $G_{I,J} \sqcup G_{I,J}$ not inducing the identity one on any of the two copies produces $| (G_{I,J} \sqcup G_{I,J})_\psi | \leq \frac{1}{N}$, since the number of these pairings is less than the total number of pairings of the Δ -labelled vertices of $G_{I,J} \sqcup G_{I,J}$, which is $(2(|I| + |J|))!!$. Then the inequality would hold with $\kappa = 2C^4$ since from the definition of *product-graph*, we see that the bound

$$| (G_{I,J} \sqcup G_{I,J})_\psi | \leq \frac{1}{N^2} \frac{1}{N^{2\frac{|I|+|J|}{2}}} N^{V_\psi} C^{2(|I|+|J|)} \quad (19)$$

must hold, where V_ψ is the number of vertices in $(G_{I,J} \sqcup G_{I,J})_\psi$. Thus it suffices to show $V_\psi \leq |I| + |J| + 1$.

To see this notice that in any case $V_\psi \leq |I| + |J| + 2$ and that $V_\psi = |I| + |J| + 2$ iff ψ identifies the random vertices in pairs. Once again there are special vertices which are not paired, the “middle” ones, the sub-graphs containing them correspond to the matrix $HH^\top = NI_N$ and can thus be removed by identifying the adjacent vertices and taking the N factor out, so these vertices must be paired between themselves, and so on. This shows that ψ has to separately pair both copies of $G_{I,J}$ in $G_{I,J} \sqcup G_{I,J}$ with identity pairings, but then such a ψ would not be an *atom-free* pairing! Hence such a ψ cannot exist and $V_\psi \leq |I| + |J| + 1$ always holds. \square

Remark A.5. Just as in the sparse case, and following [17, Section 6.1], it is possible to prove that the Δ matrices can be taken to have i.i.d. entries drawn from a centered, symmetric, but possibly heavy-tailed distribution, provided that the even moments are finite. This distributional adjustment is a useful technique for controlling the eigenvalue distribution of $\frac{1}{\sqrt{N}} H \text{diag}(\Delta)$, ensuring it has favourable computational properties while providing a theoretical guarantee of preserving expressive power.

A.4 Block Diagonal

Proposition A.6. *The sequence of triplets $(\mathcal{A}_N, \mathbb{R}^N, \mathbb{P}_N)$ where \mathcal{A}_N and \mathbb{P}_N are such that*

- $\mathcal{A}_N := \{\text{BlockDiag}(B_1, B_2, \dots, B_{k_N}) : b_N = \lceil \log(N) \rceil, k_N = \lceil N/b_N \rceil, B_h \in \mathbb{R}^{k_N b_N}\}$,
- *the initial value has independent standard Gaussian entries $[h_0]_\alpha \stackrel{\text{iid}}{\sim} \mathcal{N}(0, 1)$,*
- *the weight matrices are distributed as $[B_i]_{\alpha, \beta} \stackrel{\text{iid}}{\sim} \frac{1}{\sqrt{b_N}} \mathcal{N}(0, 1)$.*

achieves maximal probabilistic expressivity for compact sets.

Proof. Following Cirone et al. [18, Section B.3.5], we only need to prove a bound of type

$$\left\| \frac{1}{N} \langle A_I h_0, A_J h_0 \rangle_{\mathbb{R}^N} - \delta_{I,J} \right\|_{L^2(\mathbb{P}_N)} \leq (\kappa(|I| + |J|))!! \mathcal{O}(1). \quad (20)$$

It suffices to notice that

$$\frac{1}{N} \langle A_I h_0, A_J h_0 \rangle_{\mathbb{R}^N} = \frac{1}{k_N} \sum_{l=1}^{k_N} \frac{1}{b_N} \langle B_l^I h_{0;l}, B_l^J h_{0;l} \rangle_{\mathbb{R}^{b_N}}$$

where $h_{0;l} := [h_0]_{(l-1)b_N+1, \dots, lb_N}$, since we then know that

$$\left\| \frac{1}{b_N} \langle B_l^I h_{0;l}, B_l^J h_{0;l} \rangle_{\mathbb{R}^{b_N}} - \delta_{I,J} \right\|_{L^2(\mathbb{P}_N)} \leq (\kappa(|I| + |J|))!! \mathcal{O}(\frac{1}{\sqrt{b_N}}). \quad (21)$$

From the sum and the initial factor $\frac{1}{k_N}$ we obtain

$$\left\| \frac{1}{N} \langle A_I h_0, A_J h_0 \rangle_{\mathbb{R}^N} - \delta_{I,J} \right\|_{L^2(\mathbb{P}_N)} \leq (\kappa(|I| + |J|))!! \mathcal{O}\left(\frac{1}{\sqrt{b_N}}\right). \quad (22)$$

□

B Log Linear Neural Controlled Differential Equations

Combining Neural Controlled Differential Equations (NCDEs) with the Log-ODE method has been shown to produce state-of-the-art performance on a range of multivariate time series modelling benchmarks [12, 62, 91]. The same approach can be applied to Linear NCDEs (LNCDEs), and we refer to this approach as Log-LNCDEs. For a full introduction to the Log-NCDE method see [11, Section 3.2.2] and [91]. Here, we briefly outline the application of the Log-ODE method to an LNCDE, assuming familiarity with the tensor product \otimes and tensor algebra.

Recall the LNCDE model (4),

$$h_t = h_{t_0} + \int_{t_0}^t \sum_{i=1}^{d_\omega} A_\theta^i h_s d\omega_s^i, \quad (23)$$

where A_θ^i is the linear vector field for each channel and ω_s^i are the channels of our control. The log-signature of ω on $[s, t]$ is

$$\log(S(\omega)_{[s,t]}) = \log(1 + \mathbf{x}) = \sum_{n=1}^{\infty} \frac{(-1)^n}{n} \mathbf{x}^{\otimes n} \in \mathfrak{L}(\mathbb{R}_\omega^d), \quad (24)$$

where $\mathbf{x} = (0, S^1(\omega)_{[s,t]}, S^2(\omega)_{[s,t]}, \dots)$, $S^j(\omega)_{[s,t]}$ is the collection of all signature components with words of length j , and $\mathfrak{L}(\mathbb{R}_\omega^d)$ is the free Lie algebra generated by \mathbb{R}_ω^d [13, 72]. From now, we consider the log-signature truncated at level N ,

$$\log(S^N(\omega)_{[s,t]}) = (0, S^1(\omega)_{[s,t]}, \dots, S^N(\omega)_{[s,t]}), \quad (25)$$

which lives in the truncated free Lie algebra $\mathfrak{L}^N(\mathbb{R}_\omega^d)$. A basis for the truncated free Lie algebra is the Hall basis, which consists of up to the $(N-1)^{\text{th}}$ iterated Lie brackets of the basis of \mathbb{R}_ω^d , denoted $\{e_k\}_{k=1}^{d_\omega}$, where the product is the tensor product [36]. Let $\{\hat{e}_k\}_{k=1}^{\beta(d_\omega, N)}$ denote the Hall basis of the truncated free Lie algebra, where $\beta(d_\omega, N)$ is the dimension of the truncated log-signature, and let λ_k be the corresponding components of the log-signature.

Since $\mathfrak{L}^N(\mathbb{R}_\omega^d)$ is the truncated free Lie algebra, the linear map from the increments of the control to the linear ODE in (23) defined by

$$\sum_{i=1}^{d_\omega} A_\theta^i d\omega_s^i \quad (26)$$

extends to a Lie algebra homomorphism acting on the log-signature of ω defined by

$$\sum_{i=1}^{\beta(d_\omega, N)} \bar{A}_\theta^k \lambda_k, \quad (27)$$

with

$$\bar{A}_\theta^k = A_\theta^k \quad (28)$$

for $1 \leq k \leq d_\omega$ and

$$\bar{A}_\theta^k = [\bar{A}_\theta^i, \bar{A}_\theta^j] = \bar{A}_\theta^i \bar{A}_\theta^j - \bar{A}_\theta^j \bar{A}_\theta^i \quad (29)$$

when the basis element \hat{e}_k corresponds to the lie bracket of \hat{e}_i and \hat{e}_j [72]. Similarly to a Log-NCDE, the Log-ODE method is applied to (23) over intervals $t_0 = r_0 < \dots < r_m = t_n$ with $m < n$, such that

$$d\tilde{h}_s = \frac{\left(\sum_{k=1}^{\beta(d_\omega, N)} \bar{A}_\theta^k \lambda_k^l \right) \tilde{h}_s}{t_{r_{l+1}} - t_{r_l}}, \quad (30)$$

for $s \in [r_l, r_{l+1}]$, where

$$\log(S^N(\omega)_{[r_l, r_{l+1}]}) = \sum_{k=1}^{\beta(d_\omega, N)} \lambda_k^l \hat{e}_k. \quad (31)$$

The approximate solution is given by

$$\tilde{h}_{r_{l+1}} = \exp \left(\sum_{k=1}^{\beta(d_\omega, N)} \bar{A}_\theta^k \lambda_k^l \right) \tilde{h}_{r_l}, \quad (32)$$

and applying an associative scan has a reduced I/O cost as only $m < n$ state-transition matrices need to be materialised in GPU memory, as discussed in Section 4.6.

When applying the Log-ODE method to a LNCDE, the Lie brackets are calculated using the products of the linear vector fields for each channel, as opposed to the forward-mode auto-differentiated Jacobian-vector products of the vector field for Log-NCDEs. This significantly reduces the computational cost. For SLiCEs, the Log-ODE method is most beneficial when the linear ODE produced has the same vector field structure as the original vector fields. This is true for both diagonal and block-diagonal SLiCEs. Hence, in Section 5.3 and Appendix D.3, we consider diagonal, block-diagonal, and dense Log-LNCDEs.

C Matrix-valued Hidden States

LNCDEs with vector-valued hidden states are the focus of this paper. However, several LRNNs, including DeltaNet [77, 93] and Mamba [34], utilise matrix-valued hidden states. LNCDEs can be generalised to matrix-valued hidden states via

$$H_t = H_{t_0} + \int_{t_0}^t \left(\sum_{i=1}^{d_\omega} A_\theta^i d\omega_s^{X,i} \right) H_s, \quad (33)$$

where $H_s \in \mathbb{R}^{d_h \times n}$. This formulation runs n copies of the same LNCDE, with the output of each differing only due to their initial conditions. Clearly, n copies of a vector-valued LNCDE or SLiCE match the expressivity of a single copy, so all of our theoretical results naturally carry over to this setting. To introduce meaningful column-specific dynamics, LRNNs like Mamba and DeltaNet include a column-specific bias term in the vector field. A natural way to incorporate such biases into a matrix-valued LNCDE is to consider

$$H_t = H_{t_0} + \int_{t_0}^t \left(\sum_{i=1}^{d_\omega} A_\theta^i d\omega_s^{X,i} \right) H_s + B_\theta \text{diag}(d\xi_s^X), \quad (34)$$

where $B_\theta \in \mathbb{R}^{d_h \times n}$ and $\xi^X : [0, T] \rightarrow \mathbb{R}^n$ is a path, dependent on the input X . Letting h_t^k for $1 \leq k \leq n$ denote the columns of H_t , then

$$h_t^k = h_{t_0}^k + \int_{t_0}^t \left(\sum_{i=1}^{d_\omega} A_\theta^i d\omega_s^{X,i} \right) h_s^k + B_\theta^k d\xi_s^{X,k}. \quad (35)$$

Approximating ω_s and ξ_s with linear interpolation on the grid $0 = t_0 < \dots < t_n = T$ yields

$$\tilde{h}_{t_{j+1}}^k \approx \exp \left(\sum_{i=1}^{d_\omega} A_\theta^i (\omega_{t_{j+1}}^{X,i} - \omega_{t_j}^{X,i}) \right) \tilde{h}_{t_j}^k + B_\theta^k (\xi_{t_{j+1}}^{X,k} - \xi_{t_j}^{X,k}), \quad (36)$$

where we have approximated

$$\left(\sum_{i=1}^{d_\omega} A_\theta^i (\omega_{t_{j+1}}^{X,i} - \omega_{t_j}^{X,i}) \right)^{-1} \left(\exp \left(\sum_{i=1}^{d_\omega} A_\theta^i (\omega_{t_{j+1}}^{X,i} - \omega_{t_j}^{X,i}) \right) - I \right) \approx I, \quad (37)$$

for small $t_{j+1} - t_j$. The outputs $\tilde{h}_{t_j}^k$ remain computable in $\mathcal{O}(\log(n))$ parallel steps using an associative parallel scan [8].

D Additional experimental details and results

Single runs for all experiments can be completed on a 24GB NVIDIA RTX 4090 GPU in less than 24 hours. We use the following publicly available datasets, libraries, and baseline models:

- **A_5 Benchmark** [59]. License: MIT.
URL: <https://github.com/jopetty/word-problem>
- **Formal Language Benchmark** [27]. License: CC-BY-4.0.
URL: <https://arxiv.org/abs/2207.02098>
- **UEA Multivariate Time Series Classification Archive** [4]. License: GPL-3.0.
URL: <https://www.timeseriesclassification.com/>, <https://github.com/time-series-machine-learning/tsml-repo>
- **Mamba** [34]. License: Apache 2.0.
URL: <https://github.com/state-spaces/mamba>
- **DeltaNet, Gated DeltaNet, DeltaProduct** [77, 93, 94, 80]. License: MIT.
URL: <https://github.com/fla-org/flash-linear-attention>
- **xLSTM / mLSTM / sLSTM** [6]. License: Apache 2.0.
URL: <https://github.com/NX-AI/xlstm>
- **RWKV-7** [69]. License: Apache 2.0.
URL: <https://github.com/BlinkDL/RWKV-LM>
- **Log-NCDE** [91]. License: CC-BY-4.0
URL: <https://github.com/Benjamin-Walker/log-neural-cdes>
- **JAX** [10]. License: Apache 2.0.
URL: <https://github.com/google/jax>
- **PyTorch** [68]. License: BSD Style, see here <https://github.com/pytorch/pytorch?tab=license-1-ov-file>
URL: <https://github.com/pytorch/pytorch>

D.1 The A_5 benchmark

The A_5 benchmark examines a model’s state-tracking ability by asking the model to compose a sequence of even permutations on five elements [59]. There are 60 elements in the group, and the task is to compose between 3 and 20 elements. Our experiments follow the approach of Merrill et al. [59]. Models are trained using a token-tagging loss for 100,000 steps with a batch size of 256. For all sequence lengths, a small batch of sequences of length 2 are included at each training step to aid convergence. All models use Adam [49] with weight decay as their optimiser, and linear warm-up followed by cosine annealing with a minimum learning rate of 10^{-5} and a maximum learning rate of 10^{-3} . Additionally, all models use dropout [82] with a rate of 0.1 and a trainable embedding layer.

The baseline models (Mamba, LSTM, mLSTM, sLSTM, and DeltaProduct) all use a hidden dimension of 1024. LSTM uses direct stacking whereas the other baseline models use stacked blocks consisting of a sequence model, a GLU layer [26], and layer normalisation [3]. DeltaProduct uses both gating and negative eigenvalues [94, 33]. All of the SLiCEs use

$$\frac{\omega_{t_{j+1}}^X - \omega_{t_j}^X}{t_{j+1} - t_j} = (1, X_{t_j}) \quad (38)$$

and 1024 non-zero parameters for each A_θ^i . For the diagonal and Walsh–Hadamard SLiCE this corresponds to a hidden dimension of 1024 and for the dense SLiCE this corresponds to a hidden dimension of 32. The DPLR SLiCE uses a rank of 2, giving a hidden dimension of 205, and the block-diagonal SLiCE uses $b_i = 4$, giving a hidden dimension of 128. The sparse SLiCE uses a hidden dimension of 128 and a sparsity of $\epsilon = \frac{3}{7}$. All SLiCEs use stacked blocks consisting of a SLiCE, a linear layer followed by a tanh activation function, and layer normalisation. Due to issues with convergence, Walsh–Hadamard’s diagonal matrix D_θ^i is parametrised to take values between -1 and 1 .

For models with the same hidden dimension, an alternative to comparing the number of stacked layers required, as shown in Figure 1, is to evaluate the number of parameters needed to successfully

Model	Number of Parameters
LSTM	2,162,748
sLSTM	6,362,172
mLSTM	25,503,828
Mamba	26,531,260
DeltaProduct	69,609,580
D-LNCDE	12,724,284
WH-LNCDE	4,323,388

Table 4: Number of parameters for LSTM, sLSTM, mLSTM, Mamba, DeltaProduct, diagonal LNCDE (D-LNCDE), and Walsh–Hadamard LNCDE (WH-LNCDE) needed to achieve greater than 90% validation accuracy on sequences of length 20 from the A_5 benchmark when using a hidden dimension of 1024.

train on sequences of length 20, as shown in Table 4. The recurrent LSTM and sLSTM, as well as the Walsh–Hadamard LNCDE, all need only one layer, resulting in far fewer parameters than the other models. DeltaProduct has a more complex state-transition matrix than diagonal LNCDE or Mamba and still requires four layers, leading to the highest number of parameters.

D.2 Regular language tasks

Delétang et al. [27] introduced four regular language tasks as part of the formal language benchmark:

1. **Cycle navigation.** Infer the final position of a walk on a cycle starting at the origin. Actions are randomly sampled from “go forward one step”, “stay in the same place”, and “go backward one step”. We use a cycle of length 5, therefore a random guesser will achieve an accuracy of 20%.
2. **Even pairs.** There are two states in the system and the goal is to determine if there is an equal (“even”) number of transitions between the two states. As each sequence is either “even” or not, a random guesser will achieve an accuracy of 50%.
3. **Modular arithmetic (no brackets).** Performs modular arithmetic without any brackets, i.e. only handling addition and multiplication. We use mod 5 and hence a random guesser will achieve 20%.
4. **Parity.** There are two elements in the system. To determine the parity, the number of the second element is counted to determine if it is even or odd. This can be viewed as modular summation with mod 2. A random guesser achieves 50%.

This benchmark tests the ability of models to length generalise on state-tracking tasks, by training models on sequences from length 3 to 40 and evaluating models on sequences from length 40 to 256. Following Beck et al. [6], all baseline models use two stacked layers and a trainable embedding layer. In addition to the hidden dimension of 512 used by Beck et al. [6], we also train the baseline models with a hidden dimension of 128, selecting the value that yields the highest average validation accuracy for each model on each task. For Mamba, which does not support a hidden dimension of 128, we instead choose between 256 and 512 based on validation performance. All models are trained using a token-tagging loss for 100,000 steps with a batch size of 256, except for DeltaProduct which uses a batch size of 128 due to computational constraints. All models use Adam [49] with weight decay as their optimiser, and linear warm-up followed by cosine annealing with a minimum learning rate of 10^{-5} and a maximum learning rate of 2×10^{-3} . Additionally, all models use dropout [82] with a rate of 0.01 and a trainable embedding layer.

Similarly to the A_5 benchmark, LSTM uses direct stacking whereas the other baseline models use stacked blocks consisting of a sequence model, a GLU layer [26], and layer normalisation [3]. The baseline models considered are vanilla DeltaNet [77, 92], DeltaNet with negative eigenvalues (DeltaNet[-1,1]) [33], Gated DeltaNet [94], Gated DeltaProduct with negative eigenvalues and a rank of 2, sLSTM [6], mLSTM [6], xLSTM [6], RWKV-7 [69], a Transformer [89], and Mamba [34].

Table 5: Average and standard deviation of validation accuracy over five runs for a range of SLiCEs on the formal language tasks.

Model	Cycle Nav.	Even Pairs	Mod Arith. No Brack.	Parity	Average
D-LNCDE	73.4 ± 4.7	100.0 ± 0.0	20.8 ± 0.3	91.9 ± 14.5	71.5
WH-LNCDE	66.7 ± 7.9	87.5 ± 17.2	23.9 ± 1.3	62.1 ± 2.2	60.1
BD-LNCDE $_{d_h=256, b=2}$	99.2 ± 1.5	75.8 ± 12.6	41.1 ± 6.6	93.4 ± 13.9	77.4
BD-LNCDE $_{d_h=128, b=4}$	100.0 ± 0.0	91.3 ± 12.2	45.6 ± 7.8	88.4 ± 13.9	81.3
BD-LNCDE $_{d_h=64, b=8}$	93.9 ± 7.7	92.8 ± 8.2	63.9 ± 14.2	59.9 ± 8.7	77.6
BD-LNCDE $_{d_h=32, b=16}$	97.8 ± 2.3	100.0 ± 0.0	57.8 ± 32.2	50.7 ± 0.3	76.6
D-DE-LNCDE $_{d_h=510, b=2}$	69.5 ± 17.2	99.4 ± 1.2	21.0 ± 0.3	100.0 ± 0.1	72.5
D-DE-LNCDE $_{d_h=500, b=4}$	86.4 ± 30.4	85.5 ± 17.2	20.9 ± 0.3	86.6 ± 12.0	69.9
D-DE-LNCDE $_{d_h=456, b=8}$	68.5 ± 16.2	85.0 ± 11.2	39.7 ± 11.9	82.6 ± 9.9	69.0
D-DE-LNCDE $_{d_h=272, b=16}$	77.3 ± 21.3	81.4 ± 9.9	94.5 ± 5.2	81.0 ± 18.1	83.6
DPLR-LNCDE $_{d_h=171, r=1}$	44.4 ± 10.5	70.8 ± 15.8	24.6 ± 5.1	74.9 ± 23.7	53.7
DPLR-LNCDE $_{d_h=102, r=2}$	34.8 ± 16.7	68.1 ± 4.5	26.5 ± 1.2	79.9 ± 20.5	52.3
DPLR-LNCDE $_{d_h=57, r=4}$	83.9 ± 20.1	97.7 ± 5.2	26.0 ± 0.7	79.6 ± 20.3	71.8
DPLR-LNCDE $_{d_h=30, r=8}$	79.9 ± 14.7	94.1 ± 6.0	27.5 ± 3.5	72.6 ± 15.6	68.5
Random	20.0	50.0	20.0	50.0	35.0

We consider all SLiCEs on this benchmark except sparse due to the lack of an efficient implementation. All SLiCEs use

$$\frac{\omega_{t_{j+1}}^X - \omega_{t_j}^X}{t_{j+1} - t_j} = (1, X_{t_j}), \quad (39)$$

and two stacked blocks consisting of the sequence layer, a linear layer followed by a tanh activation function, and layer normalisation. For the diagonal and Walsh–Hadamard SLiCE variants, we consider hidden dimensions of 128 and 512, corresponding to 128 and 512 non-zero parameters per state-transition matrix, respectively. For all other SLiCE variants, the number of non-zero parameters in the state-transition matrix is fixed at 512. For DPLR we consider ranks of $r = 1, 2, 4, 8$, and for block-diagonal we consider two variants, $b_i = b$ for all i with $b = 2, 4, 8, 16$, and $b_i = 1$ for $i = 1, \dots, k-1$, and then a final dense block $b_k = b$ for $b = 2, 4, 8, 16$, referred to as diagonal-dense LNCDE (D-DE-LNCDE). Due to issues with convergence, Walsh–Hadamard’s diagonal matrix D_θ^i is parametrised to take values between -1 and 1 .

Table 5 presents the average validation accuracy for all the SLiCE variants. Despite improving performance on the A_5 benchmark, replacing the diagonal LNCDE with a Walsh–Hadamard LNCDE leads to a worse average validation accuracy on the regular language tasks. A key reason is the poor performance of Walsh–Hadamard LNCDE on parity. For a fixed block-size block-diagonal LNCDE, any $b_i > 1$ leads to improved average validation accuracy over a diagonal LNCDE. In particular, the performance peaks at $b_i = 4$, providing empirical evidence that for a fixed computational budget (or number of non-zero state-transition parameters), there is a trade-off between expressivity and hidden dimension. Using a diagonal-dense LNCDE allows for a larger hidden state whilst having a dense block, and the largest dense block, $b = 16$, has the best average validation accuracy of any model considered in this paper. Unlike block-diagonal, replacing the diagonal LNCDE with a DPLR-LNCDE yields only a minor improvement in average validation accuracy for $r = 4$, with all other choices for r decreasing the average validation accuracy. However, gated DeltaProduct with negative eigenvalues and a rank of 2 is the best-performing baseline model, showing that DPLR structures are capable of performing well at length-generalisation on state-tracking tasks. We believe the discrepancy between gated DeltaProduct and DPLR-LNCDE is due to not adjusting the hidden dimension of baseline models to account for increased complexity in the state-transition matrices, meaning gated DeltaProduct has over 8 times as many parameters as DeltaNet.

D.3 UEA multivariate time series classification archive

The experiments on the UEA multivariate time series classification archive follow the approach of Walker et al. [91], including the same hardware and data splits. In order to ensure stability, the datasets were normalised and the log-signatures scaled down by a factor of ten on Heartbeat. The diagonal, block-diagonal, and dense LNCDEs all use identical hyperparameters to the Log-NCDE, but replace

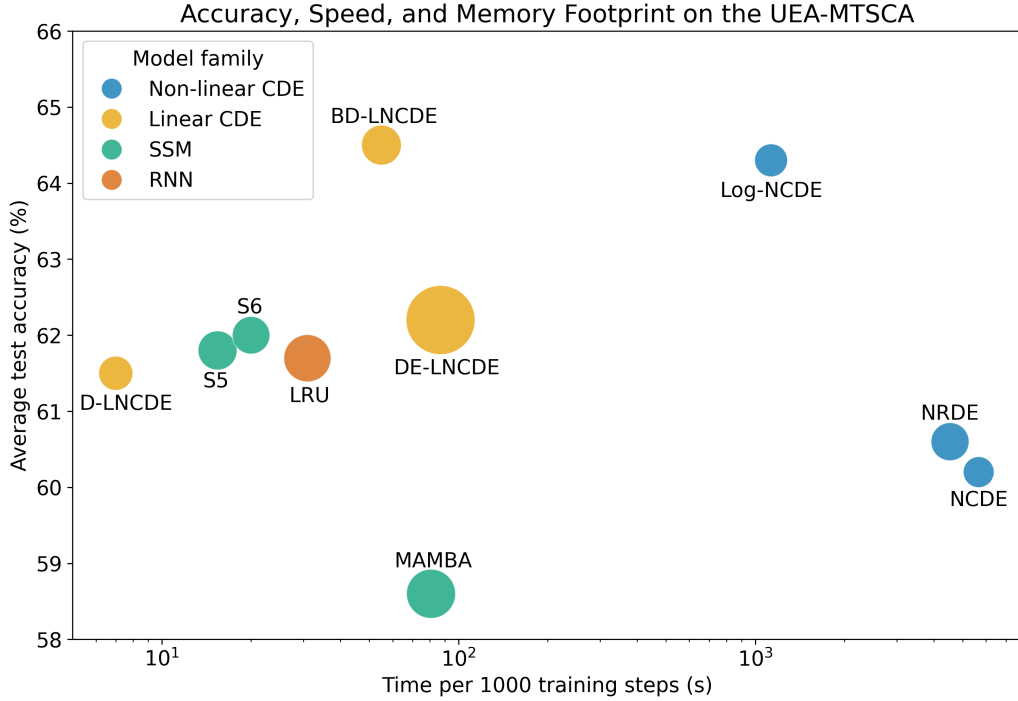


Figure 5: Average per-step training time versus average validation accuracy across six multivariate time-series classification datasets from the UEA-MTSCA. Each point represents a model, with circle area proportional to average GPU memory usage. We compare four families of models: a recurrent neural network (LRU), SSMs (S5, S6, and Mamba), non-linear NCDEs (NCDE, NRDE, and Log-NCDE), and linear NCDEs (Diagonal LNCDE, Block-Diagonal LNCDE, and Dense LNCDE). All results except linear NCDEs are from Walker et al. [91].

the non-linear vector field with their respective structured linear vector fields. The Log-ODE method is applied over the same intervals as for the Log-NCDE, and an associative parallel scan is used to compose the output from the Log-ODE method on each interval. All the SLiCEs take $\omega_s^X = X_s$.

Figure 5 expands on the results in Table 3, by including the results for S5 [81], the linear recurrent unit (LRU) [66], Mamba [34], neural controlled differential equation (NCDE) [48], and neural rough differential equation (NRDE) [63] from Walker et al. [91]. Despite Log-NCDEs improving on the average training time per step of NCDEs and NRDEs, there is still a large gap between S5, S6, LRU, and Mamba.

Replacing the non-linear vector field with a block-diagonal linear vector field reduces the average time per training step by a factor of 20, bringing the model within the range of per-step training time of the SSM baselines, without impacting the average test accuracy. The training time can be reduced even further by using a diagonal linear vector field, but this reduces the average test accuracy on all six datasets, possibly due to the decreased expressivity. Using a dense linear vector field increases the run-time and GPU memory compared to a block-diagonal linear vector field. Additionally, it decreases the average test accuracy on all six datasets, possibly due to over-fitting from the large number of parameters per state-transition. These results suggest that using a block-diagonal linear vector field may have benefits beyond simply reducing the computational cost of the model.